AD NUMBER: AD0480801
LIMITATION CHANGES
TO: Approved for public release; distribution is unlimited.
FROM: This document is subject to special export controls; 01 Jan 1966, and each transmittal to foreign goverments or foreign nationals may be made only prior approval of Metals and Ceramics Division, Air Force Materials Laboratory, Wright-Patterson Air Force Base, Ohio, 45433.
AUTHORITY
ST-A PER AFSC/IST(WPAFB,OH)Ltr dtd 21 Mar 1989

AD NUMBER

480 801

CLASSIFICATION CHANGES

TO

FROM

AUTHORITY

WRDC / 1st L TR dtd 21 MAR 89
(For Entries 11 thru)

AFML-TR-65-2
Part II, Volume IV.

TERNARY PHASE EQUILIBRIA IN TRANSITION METAL-BORON-CARBON-SILICON SYSTEMS

Part II. Ternary Systems

Volume IV. The Ti-Zr-C, Ti-Hf-C and Zr-Hf-C Systems

C. E. Brukl
D. P. Harmon

Aerojet-General Corporation

TECHNICAL REPORT NO. AFML-TR-65-2, PART II, VOLUME IV

January 1966

Air Force Materials Laboratory
Research and Technology Division
Air Force Systems Command
Wright-Patterson Air Force Base, Ohio

TERNARY PHASE EQUILIBRIA IN TRANSITION METAL-BORON-CARBON-SILICON SYSTEMS.

Part II. Ternary Systems.

Volume IV. The Ti-Zr-C, Ti-Hf-C, and Zr-Hf-C Systems.

C. E. Brukl
D. P. Harmon.

This document is subject to special export controls, and each transmittal to foreign governments or foreign nationals may be made only with prior approval of Metals and Ceramics Division, Air Force Materials Laboratory, Wright-Patterson Air Force Base, Ohio.

FOREWORD

The work described and illustrated in this report was performed at the Materials Research Laboratory, Aerojet-General Corporation, Sacramento, California under USAF Contract No. AF 33(615)-1249. The contract was initiated under Project No. 7350, Task No. 735001. The work was administered under the direction of the Air Force Materials Laboratory, Research and Technology Division with Captain R. A. Peterson and Lt. P.J. Marchiando acting as Project Engineers, and Dr. E. Rudy, Aerojet-General Corporation, as Principal Investigator. Professor Dr. Hans Nowotny, University of Vienna, Austria, served as consultant to the project.

The project, which includes the experimental and theoretical investigation of selected refractory ternary systems in the system classes Me_1-Me_2-C, Me-B-C, Me_1-Me_2-B, Me-Si-B, and Me-Si-C was initiated on 1 January 1964.

The experimental program was laid out by E. Rudy, and the authors wish to acknowledge the many helpful hours given by Dr. E. Rudy to aid in the interpretation of experimental results. J. Hoffman, R. Radtke, R. Cobb and J. Pomodoro were of valuable assistance in the preparation of the experimental work.

Chemical analyses of the alloys was carried out under the supervision of Mr. W. E. Trahan, Metals and Plastics Chemical Testing Laboratory, Aerojet-General Corporation. The writers also wish to thank Mr. R. Cristoni, who prepared the many drawings, and Mrs. J. Weidner who typed the report.

The manuscript of this report was released by the authors in September 1965 for publication as an RTD Technical Report.

Other reports issued under USAF Contract AF 33(615)-1249 have included:

Part I. Related Binaries

- Volume I. The Mo-C System
- Volume II. The Ti-C and Zr-C Systems
- Volume III. The Mo-B and W-B Systems
- Volume IV. The Hf-C System
- Volume V. The Ta-C System, Partial Investigations in the Nb-C and V-C Systems

Part II. Ternary Systems

- Volume I. The Ta-Hf-C System
- Volume II. The Ti-Ta-C System
- Volume III. The Zr-Ta-C System

FOREWORD (Cont'd)

Part III. Special Experimental Techniques

Volume I. High Temperature Differential Thermal Analysis

Part IV. Thermochemical Calculations

Volume I. Thermodynamic Properties of Group IV, V, and VI Binary Transition Metal Carbides.

This technical report has been reviewed and is approved.

W. G. RAMKE
Chief, Ceramics and Graphite Branch
Metals and Ceramics Division
Air Force Materials Laboratory

ABSTRACT

Solid-state sections of the ternary Ti-Zr-C and Ti-Hf-C systems were investigated; the complete Zr-Hf-C system was studied from 1600°C to melting using X-ray, DTA, melting point, and metallographic techniques on chemically analyzed alloys; a complete phase diagram for the Zr-Hf-C system for temperatures above 1600°C was established. The hafnium metal used contained 4 At. % zirconium.

The Ti-Zr-C system contains a miscibility gap in the monocarbide region; the miscibility gap is completely closed at temperatures above approximately 2150°C.

A miscibility gap is also present in the Ti-Hf-C system in the monocarbide region; complete solid solubility exists between the binary monocarbides at temperatures above approximately 2050°C.

The Zr-Hf-C system contains a high melting, continuous monocarbide solid-solution in a carbon defect lattice. The α-hafnium phase is stabilized toward higher temperatures by carbon; this phase shows a moderate solubility for carbon and zirconium.

One four-phase reaction plane is present in the metal-rich portion of the ternary diagram.

The results of these investigations are described and discussed; application possibilities are briefly mentioned.

TABLE OF CONTENTS

TABLE OF CONTENTS (Cont.)

ILLUSTRATIONS

ILLUSTRATIONS (Cont.)

ILLUSTRATIONS (Cont.)

ILLUSTRATIONS (Cont.)

TABLES

I. INTRODUCTION AND SUMMARY

A. INTRODUCTION

The ternary systems Ti-Zr-C, Ti-Hf-C, and Zr-Hf-C have received relatively little attention except for crystal structural investigations in the monocarbide regions. Part of the lack of interest in these systems is due to the fact that titanium possesses the lowest melting point of all the refractory metals. The past and present prohibitively high price of hafnium has almost prevented consideration of this metal and its alloys for possible extensive commercial applications, and because of this, there has been relatively little research done with hafnium although many of its alloys and compounds belong to the most refractory materials known.

Zirconium, along with its alloys and compounds, has commanded a high position in research of nuclear-application materials because of its unusually small neutron capture cross-section. Refractory combinations of zirconium, and its compounds, with other refractory metals will play a leading role in our present Space and Nuclear Age.

The cutting tool industry in the United States has been manufacturing products based on WC-TiC-TaC mixtures with iron group metals as binders; detailed information concerning other refractory alloy-carbide combinations was therefore not particularly necessary for the production of these types of cutting tools. There has been little directed interest in the improvement of cutting speeds and temperatures of materials based on refractory metals as binders, although refractory composites show promise of increasing cutting speed and temperature by virtue of their higher melting points.

Combinations of zirconium and hafnium carbides as well as composite bodies containing these materials would most probably not be used for nuclear applications, except for an extremely specific purpose; hafnium, in contrast to zirconium has a very high neutron capture cross-section.

However, the combination of zirconium and hafnium carbides will belong to the most refractory materials, and high temperature applications for these combinations are a distinct probability.

Not only would a detailed investigation of the Zr-Hf-C system and high temperature isotherms of Ti-Zr-C as well as Ti-Hf-C systems suggest new application possibilities for composite materials, but more important, accurately known phase equilibria relationships at high temperatures enable badly needed thermodynamic values to be obtained. These values, when obtained, used in conjunction with data available from the investigations of other carbide systems, provide valuable tools for the prediction of alloy application and behavior in ternary and higher order carbide systems.

The present investigations, therefore, were directed toward the establishment of high temperature phase equilibria, determination of the maximum solidus regions, (Zr-Hf-C) and in particular, the phase relationships in the metal-rich portions of the ternary systems. In the majority of instances, graphical presentation of data was given preference over tabular compilation.

B. SUMMARY

Isothermal sections of the Ti-Zr-C and Ti-Hf-C were investigated using X-ray and differential thermal analysis techniques. The Zr-Hf-C system was studied in its entirety with the help of melting point determinations and metallographic examinations in addition to the methods stated above.

Many of the alloys prepared were analyzed post-experimentally for their carbon content to check the nominal concentrations.

1. Binary Systems

The binary titanium-carbon, zirconium-carbon, and hafnium-carbon systems have been extensively investigated and recently described in previous reports[1, 2] (Figures 4, 5, and 7).

2. Ternary Systems

a. The Ti-Zr-C System

Lattice parameter measurements (Figures 10, 11, and 12) and DTA experiments (Figures 14 and 15) show that at 1500°C a large miscibility gap between approximately 23 and 81 Mol % ZrC exists in the monocarbide region. As a result of this miscibility gap, extended three-phase regions are present on both the carbon-rich and metal-rich sides of the monocarbide region (Figure 16).

b. The Ti-Hf-C System

Again, lattice parameter measurements (Figures 19, 20, and 21) and DTA results (Figure 22) show that at 1500°C a miscibility gap from 22 to 51 Mol % HfC exists in the carbon-rich portion of the monocarbide region (Figure 23). There is complete solid-solution between the high-carbon-defect binary monocarbides along the metal-rich boundary of the ternary monocarbide at 1500°C. The carbon-rich region of the ternary system contains the three-phase field, $(Ti, Hf)C_{1-x}$-$(Hf, Ti)C_{1-x}$-C, which results from the miscibility gap. The greater portion of the metal-rich area of the diagram is two-phased, i.e., β-(Ti, Hf)-$(Ti, Hf)C_{1-x}$. On the hafnium-rich side of the ternary, the above mentioned two-phase region is interrupted by a narrow three-phase, β-(Hf, Ti)-α-(Hf, Ti)-$(Hf, Ti)C_{1-x}$, area

rising from Ti-Hf binary, at 1500°C the $\alpha \rightleftarrows \beta$ transformation is located at about 82 At.% Hf. The extreme hafnium-rich portion of the ternary is characterized by a $(Hf, Ti)C_{1-x}$ - α-(Hf, Ti) two-phase equilibria.

c. The Zr-Hf-C System (Figure 56)

(1) Monocarbide Region

The face-centered, cubic binary phases $ZrC_{.98}$(a = 4.700 Å) and $(Hf_{.98}Zr_{.02})C$ (a = 4.640 Å) form a continuous series of solid solutions to melting; the lattice parameters of the mixed crystal show a slight negative (contraction) deviation from Vegard's Law (Figures 26 and 27). The melting points of the monocarbide solid solution decrease almost linearly from HfC_{1-x} to ZrC_{1-x} (Figures 49 and 50).

(2) Carbon-Rich Equilibria

There are no other ternary phases except the monocarbide solid-solution in this area. A monocarbide-graphite eutectic trough runs almost linearly across this region between the Hf-C binary eutectic at 65 At.% C and the Zr-C eutectic at 64.5 At.% C (Figure 58). The eutectic temperatures decrease smoothly from 3180°C on the hafnium side to 2911°C on the zirconium side (Figure 54).

(3) Metal-Rich Equilibria

One four-phase reaction plane is present in the region between the monocarbide solid-solution and the metal binary.

(a) Class II* Four-Phase Equilibrium at 2030°C (IIa in Figure 58 and 62)

The four-phase reaction occurring at this temperature is represented by the following reaction equation:

*The excellent book, Phase Diagrams in Metallurgy by F. Rhines was extensively consulted in regard to nomenclature and equilibria questions. The nomenclature proposed therein has been used in this report.

$$\text{Liquid} + \alpha\text{-Hf(Zr,C)} \underset{T \leq 2030°C}{\overset{T > 2030°C}{\rightleftharpoons}} (Hf, Zr)C_{1-x} + \beta\text{-(Zr,Hf)}$$

Table 1. Four-Phase Reaction Plane: Liq + α ⇄ δ + β at 2030°C
Equilibrium Concentrations of Partaking Phases

Phase	Concentrations in At. % Zr	Hf	C
Liquid	35	63.5	~1.5
α-Hf(Zr,C)	23	68.5	8.5
$(Hf, Zr)C_{1-x}$(δ)	9	53.5	37.5
β-(Hf, Zr)	35.5	64	~0.5

The homogeneous range of the hexagonal, low temperature α-form of the binary metal phase decreases along the binary with increasing temperature and eventually disappears from the metal binary at the transition temperature of α-Hf; this phase, is however, stabilized to higher temperatures by carbon and extends into the ternary from the Hf-C side and shows a moderate solubility for both carbon and zirconium (Figures 60-65).

The ternary eutectic trough, connecting the binary eutectics at approximately 1.5 At.% carbon on both the hafnium and the zirconium sides, lies very close to the binary Hf-Zr side of the ternary system (Figure 58). The metal-rich eutectic temperatures vary smoothly from 1835°C on the zirconium side to 2180° on the hafnium side.

The two-phase metal-monocarbide region is interrupted by a small three-phase, β-(Zr, Hf)-α-(Zr, Hf)-(Hf, Zr)C_{1-x} area which progresses toward the hafnium-rich side with increasing temperatures; this three-phase area vanishes at temperatures above the Class II four-phase reaction plane.

II. LITERATURE REVIEW

A. BINARY SYSTEMS

1. Metal-Metal Binaries

The group IVa metals, Ti, Zr, and Hf, undergo an alliotropic transformation at elevated temperatures; in each case the low-temperature α-form has a hexagonal, close-packed lattice, the A3 type structure[3, 4, 5]; the high-temperature β-form has a body-centered, cubic unit cell, the A2 type[5, 6, 7, 8]. Table 2 gives the transformation temperatures and melting points of the group IVa metals.

Titanium and zirconium[22, 23], titanium and hafnium[24], and zirconium and hafnium[6] form a continuous body-centered, cubic solid-solution at high temperatures and a continuous, close-packed hexagonal solid-solution at low temperatures (Figures 1, 2, and 3).

2. Metal-Carbon Binaries

a. Titanium-Carbon (Figure 4)

In the system Ti-C there exists a single intermediate phase, the monocarbide, which crystallizes in a face-centered cubic structure, the NaCl type[25]. The TiC phase has an extended homogeneous range, and at the temperature of previous investigations[1] (1500°C), the lower boundary is located at 32.5 At.% carbon (a = 4.305 Å). P. Ehrlich[26] has indicated the lower boundary to be at 22 At.% carbon; however, according to L. Stone and H. Margolin[27] this result is most likely based on oxygen

Table 2. α-β-Transformation Temperatures and Melting Points of Titanium, Zirconium, and Hafnium

Element	α-β-Transition Temp., °C	Melting Point, °C
Ti	882 [9]	1668 ± 8 [1]
		1660 [10]
	880 ± 10 [1]	1725 ± 10 [11]
		1800 [14]
Zr	865 [13]	1855 ± 15 [14]
	872 ± 15 [1]	1860 ± 15 [15]
		1876 ± 4 [1]
Hf	1310 [8]	2208 [21]
	1327 to 1527 [16]	2218 ± 6 [2]
	1750 ± 20 [17]	2222 ± 30 [11, 14]
	1777 [18]	
	1840 [19]	
	1840 ± 25 [2]	
	1950 [5]	
	1995 ± 70 [20]	

contaminated alloys. The upper limit of the monocarbide phase has been reported to be $TiC_{1.0}$ [28], $TiC_{0.95}$ [29], $TiC_{0.96}$ [1], with the respective lattice parameters being: a = 4.3280 [28], a = 4.3305 [29], and a = 4.330 Å [1].

The monocarbide phase is in equilibrium with β-titanium above ~930° [1]. I. Gadoff and J. P. Nielson[30] have found the carbon solubility in β-Ti to be 0.6 At.% (920°C), 1.1 At.% (1400°C), and

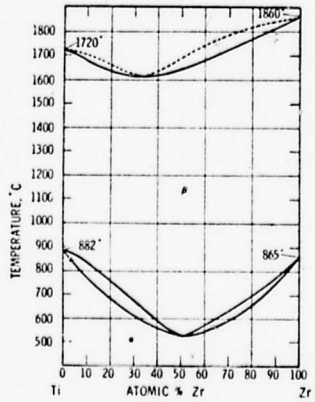

Figure 1. Ti-Zr: Constitution Diagram
(M. Hansen: Constitution of Binary Alloys, 1958)

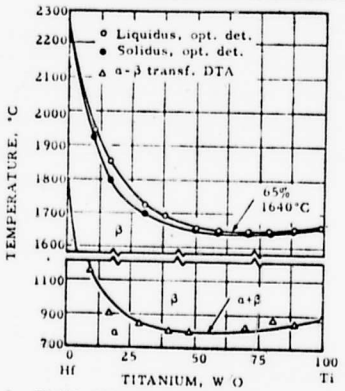

Figure 2. Ti-Hf: Constitution Diagram
(D. Thomas and E. Hayes: The Metallurgy of Hafnium, Government Printing Office)

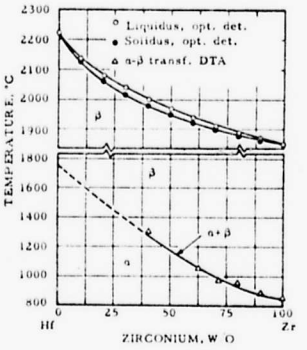

Figure 3. Zr-Hf: Constitution Diagram
(D. Thomas and E. Hayes: The Metallurgy of Hafnium, Government Printing Office

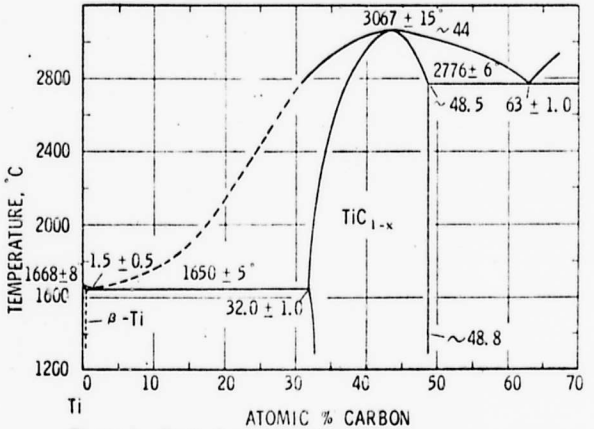

Figure 4. Ti-C: Constitution Diagram
(E. Rudy, D. Harmon, and C. Brukl, 1965)

3.1 At.% at the peritectic temperature (1750°C); however, in view of recent findings that eutectic melting actually occurs[31, 1], the carbon solubility will most likely be somewhat less at high temperatures[1].

(b) Zirconium-Carbon

Recent investigations[1] within this laboratory (Figure 5) have confirmed the Zr-C constitution diagram as determined by R.V. Sara[15].

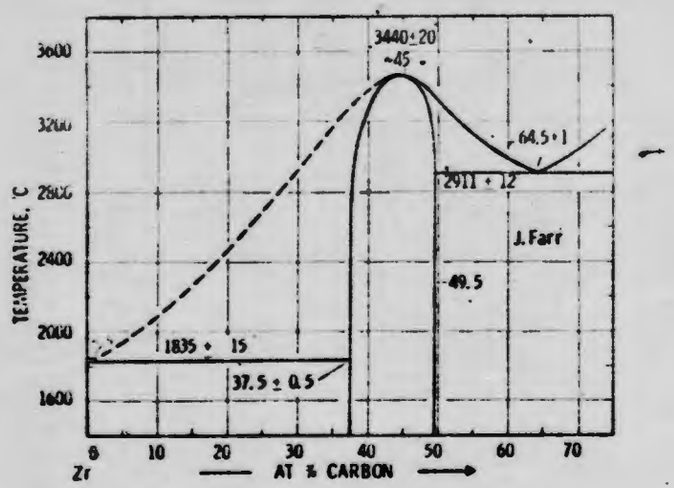

Figure 5. Zr-C: Constitution Diagram
(E. Rudy, D. Harmon, and C. Brukl, 1965)

The α-β-Zr transformation temperature in the two-phase region, $Zr-ZrC_{1-x}$, was found to be ~885°C[15] and ~875°C[1]; a

peritectoid decomposition of the α-phase is most likely to occur in view of results obtained in the Ti-C and Hf-C systems[1].

The monocarbide phase, (f.c.c.-NaCl type structure[25]) is found to have an extended range of homogeneity. The most recent determinations of the limits are: (lower): 35.4 At.% C[32], 38.5 At.% C[15], and 37.5 At.% C[1], (upper): in each case the upper limit was defined as 49.4 At.% C using the value determined by J. Farr[34]. Figure 6 gives a lattice parameter plot of samples quenched from above 2800°C[1]; the anomalous maximum has also been observed by Sara[15] in alloys heat-treated at high-temperatures (3300°C).

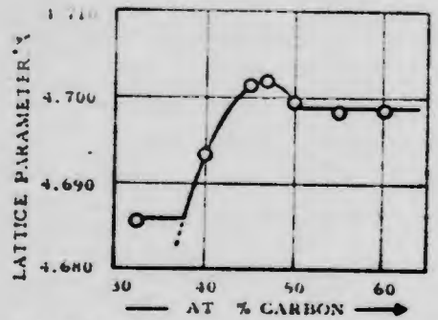

Figure 6. Zr-C: Lattice Parameters of Monocarbide Phase
(E. Rudy, D. Harmon, and C. Brukl, 1965)

The monocarbide phase melts congruently at a substoichiometric composition of approximately 45-46 At.% carbon[1, 15, 32], and at a temperature of 3400 - 3440°C[1, 15, 34].

The eutectic [illegible] and [illegible] been reported to [illegible] and 1833°C [illegible], Rara[15] locates the eutectic composition at approximately 1 At.% carbon.

For the ZrC-C eutectic temperature, literature values are: 2850°C[15], 2850 ± 50°C[32], 2911 ± 12°C[4], and 2920 ± 50°C[31]; the eutectic is located at a carbon concentration of approximately 65 atomic percent[1, 15].

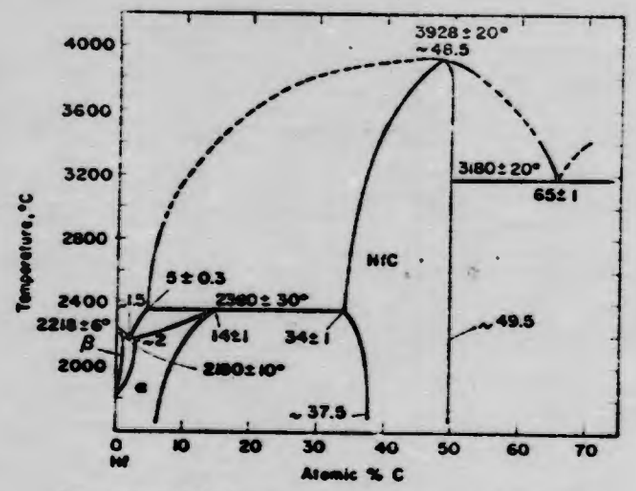

Figure 7. Hf-C: Constitution Diagram (E. Rudy, 1965)

c. Hafnium-Carbon (Figure 7)

Similar to the occurrences in the Ti-C and Zr-C binary systems, a single intermediate phase (HfC) is formed in the

[illegible] unlike the other two group-IVa metal-carbon systems, [illegible] established to much higher temperatures and carbon concentrations [illegible] incorporating carbon atoms into interstitial lattice sites[38]. The α-Hf phase decomposes peritectically into HfC_{1-x} and liquid at 2360°C and forms a eutectic with the β-Hf phase at 2180°C at approximately .5 At.% carbon[2].

The monocarbide phase (NaCl type structure[36]) has a homogeneity range between 34 At.% C (a = 4.608 Å)[2] and 49.5 At.% C (a = 4.640 Å)[2] at the peritectic and eutectic temperatures respectively. The lower boundary is strongly temperature dependent below the peritectic isotherm[2, 21]. At 1500°C the boundary is located at a carbon concentration of 37.5 atomic percent[33]. As early as 1930, the HfC_{1-x} phase was reported to have an extremely high melting point. Agte and H. Alterthum[37] found that the phase melted at 3890°C. Subsequent measurements have resulted in values 3895°C[38], 3830°C[21] and 3928°C[2] for the melting point of HfC_{1-x}; the melting point maximum is located at approximately 48.5 At.% carbon[2].

The eutectic between the monocarbide phase and carbon is located at a carbon concentration of 65-66 atomic percent; the eutectic temperature has been measured on several occasions; the following values have been published: 2800°C[34], 2915°C[39], 3150°C[21], 3180°C[2], and 3260°C[34].

B. TERNARY SYSTEMS

1. The Ti-Zr-C, Ti-Hf-C, and Zr-Hf-C Systems

Very little experimental work has been performed on systems containing the IVa group metals; the only literature information on

these systems pertains to the monocarbide solid-solutions. Above 2100°C the systems TiC-ZrC[40,41,42,43], TiC-HfC[44,45,46,47], and ZrC-HfC[44,45,46,47] were all found to form a complete series of solid solutions; however, H. Nowotny and R. Kieffer[40] found that TiC-ZrC alloys, heat treated at 1600°C for two hours, were heterogeneous and still had lattice parameters of the carbide starting products. This latter result was attributed to the slow reaction rates involved, and it was concluded that titanium and zirconium monocarbides were completely miscible at this temperature. Figure 8 gives a composite picture of the lattice parameters of the monocarbide solid solutions as presented in "Hartstoffe".[48]

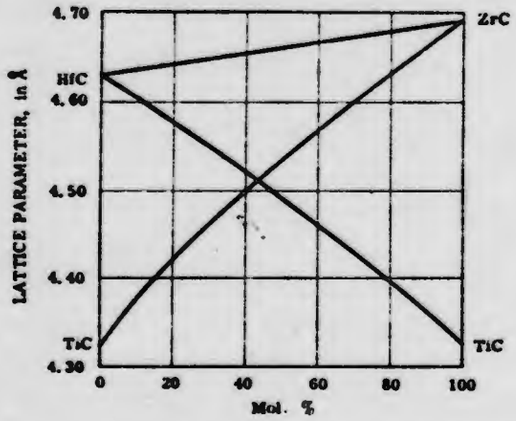

Figure 8. Lattice Parameters of Group IVa Monocarbide Solid-Solutions.
(Composite Picture: H. Nowotny, et.al., 1959, as well as J. Norton and A. Mowry, 1949)

III. EXPERIMENTAL PROGRAM

A. EXPERIMENTAL PROCEDURES

1. Starting Materials

Elemental, pre-prepared binary monocarbide, and metal hydride powders were used as the starting materials. Due to the exceptionally high price ($1362/lb.) of zirconium-free hafnium, commercial grades of hafnium containing up to 3.2 Wt.% (6.1 At.%) zirconium were used in these investigations.

Titanium metal powder was obtained from the Var-Lac-Oid Chemical Company, New York, and had the following impurities (in ppm): C-1300, H-1500, N-50, Hf-500 and Cl-1200. The lattice parameters of this starting material, as determined with CuK_α, were $a = 2.94_0$ Å and $c = 4.68_0$ Å. The particle size was smaller than 74 micrometers.

Titanium dihydride, Grade E, purchased from Metal Hydrides, Inc., Beverly, Mass., had the following impurities (in ppm): Al-1000 - 3000, C-1000 max., Ca-500 max., Fe-1000 max., Mg-500 max., N-2000 max., Si-1000 max., and Zr-1000 max.; the hydrogen content was 3.99% by weight. This titanium hydride had an average particle size of 7.3 micrometers. A Debye-Scherrer powder diagram of this material showed only the face-centered cubic dihydride structure. Spectrographic analysis at the Aerojet Metals and Plastics Chemical Testing Laboratory resulted in the following data (in ppm): Cr-400, Al-10, Fe-100, Zr-50, and Ca-100.

Zirconium metal powder was obtained from the Wah Chang Corporation, Albany, Oregon and had the following main impurities (in ppm): C-40, Nb-<100, Fe-315, Hf-67, N-34, O-830, Si-<40, Ta-<200,

Ta-20, [illegible]. The lattice parameters of this starting material were a = 3.232 Å and c = 5.149 Å. The particle size of this material was ranged between 74 and 44 micrometers. Spectrographic analysis performed at the Aerojet Metals and Plastics Chemical Testing Laboratory yielded the following results (in ppm): Si-10, Fe-20, Ta - not detected, and Hf-500. A vacuum fusion analysis performed in the same laboratory yielded these results (in ppm): O-1109, N-272, and H-739.

Zirconium dihydride, also purchased from the Wah Chang Corporation, Albany, Oregon had the following main impurities (in ppm): C-320, Nb-<100, Cr-125, Fe-1800, Hf-137, Mg-255, N-116, O-1300, Si-157, Ta-<200, Ti-29, and W-<25. The hydrogen content was 2.1% by weight, and the particle size was less than 44 micrometers. An over-exposed Debye-Scherrer powder diagram of the zirconium hydride powder showed only the tetragonal-$ZrH_{\sim 2}$-pattern with no other extraneous lines. Spectrographic analysis done at the Aerojet MPCT Laboratory yielded the following results (in ppm): Si-10, Fe-500, Ta-not detected, Hf-<100 and Mg-40.

Two different batches of hafnium powder, which were supplied by the Wah Chang Corporation, Albany, Oregon were used. The first lot contained the following main impurities (in ppm): C-210, Nb-680, Cr-<20, Fe-265, H-55, N-200, O-810, Si-<40, Ta<200, and W-235. The zirconium content was 3.2% by weight. Spectrographic analysis performed at Aerojet's MPCT Laboratories gave the following results (in ppm): C-not detected, Si-10, N-250, Nb-<1000, Ta-500, Zr->>2500, and W-not detected. The lattice parameters of this hafnium powder determined on a CuK_α pattern was a - 3.19$_6$ Å and c - 5.05$_7$ Å; the average particle size of the powder was 74 micrometers.

The second lot of hafnium powder, used in the Zr-Hf-C system investigations, had the following main impurities (in ppm): C-60, Nb-<100, Cr-<10, Fe-95, H-45, N-200, O-660, Si-<40, Ta-<200, and W-<20; the zirconium content was 2.5% by weight. The particle size of this material was smaller than 74 micrometers, and the lattice parameters as determined on a film taken with CuK_α radiation were a = 3.19$_5$ Å and c = 5.05$_5$ Å.

Hafnium hydride, supplied by the Wah Chang Corporation, Albany, Oregon had the following main impurities (in ppm): Al-80, C-50, Nb-100, Cr-<10, Fe-190, Mg-250, N-20, O-330, Si-<40, Ta-<200, Ti-75, W-<20; the material contained 1.35 Wt% zirconium and 0.92 Wt% hydrogen. The particles were sized between 250 and 74 micrometers. Spectrographic analysis gave the following values (in ppm): C-500, Si-10, Ti-40, Nb-not detected, Ta-not detected, Zr->>6000, W-300, and Mg-1000. A Debye-Scherrer powder diagram of the hydride powder showed only the tetragonal-$HfH_{\sim 2}$ pattern with no other extraneous lines.

Carbon was used in two forms. The lampblack powder, supplied by Monsanto Chemical Co., had 99.57% free carbon, and the following impurities (in ppm): H_2O-400, Benzol Extract-3000, Ash-300, and Volatiles-3600. The particle size was 0.01 - 0.1 micrometers. Spectrographic analysis at the Aerojet Metals and Plastics Chemical Testing Laboratory gave the following results (in ppm): Si-20, Mg-<10, Cu-<10, Al-10, Fe-10.

Graphite powder was obtained from the National Carbon Company and had the following typical impurities (in ppm): S-110, Si-40, Ca-44, Fe-40, Al-8, Ti-4, Mg-2, V-trace, and Ash-800 max. Ninety-nine percent of the graphite was smaller than 74 micrometers. Highly

overexposed X-ray films of these materials showed no traces of any impurity phase.

Var-Lac-Oid, Inc., New York supplied the titanium monocarbide powder. The impurities were (in ppm): Fe-500, Si-100, Ca-100, Na-50, O-1000, and N-1500. The monocarbide had a total carbon content of 19.50 Wt% C.(49.1 At.%) and 19.30 Wt% bound carbon (48.8 At.%). The lattice parameter of this starting material was 4.323 Å, and the particle size was smaller than 88 micrometers.

The zirconium monocarbide powder was purchased from the Wah Chang Corporation, Albany, Oregon. The main impurities were (in ppm): Nb-< 100, Fe-< 50, Hf-< 10, Mo-< 10, N-1100, O-1040, Si-< 40, Ta-< 200, Ti-50, and W-< 25. The monocarbide had a carbon content of 11.94 Wt% (49.8 At.%) and a particle size smaller than 44 micrometers.

2. Alloy Preparation and Heat Treatment

a. The Ti-Zr-C System

Samples for the investigation of the solid-state isotherm at 1500°C (Figure 9) were prepared by hot pressing the elemental powders and hydrides in graphite dies at temperatures between 1300° and 2300°C. Approximately 1 Wt% nickel powder was added to those samples in the monocarbide region to aid in the attainment of equilibrium. The nickel completely evaporates from the carbide samples during the ensuing heat treatments.

After being surface cleaned, the samples were heat treated for 60-64 hours at 1500°C under a protective atmosphere of helium at atmospheric pressure. After the heat treatment, a portion of each sample was powdered and an X-ray diffraction pattern using the Debye-Scherrer powder technique was made; the samples in the metal-rich region

were stress annealed for a short time. Several selected samples in the monocarbide region were subsequently heat treated at 1800° and 2100°C to ascertain the critical temperature and concentration of the large miscibility gap. In addition to some DTA samples, also prepared by hot pressing, several samples in the monocarbide region were quenched from temperatures in the range 1800 - 2100°C into a liquid tin bath to further confirm the presence and closing of the miscibility gap.

b. The Ti-Hf-C System

The alloy preparation, both for solid-state and DTA samples as well as for quenching samples, in this system followed the same steps as those described for the Ti-Zr-C system. The solid state samples (Figure 17) were heat treated at 1400°C for 51 hours under helium at atmospheric pressure. Selected samples in the monocarbide region were subsequently heat treated at 1700°C for 17 hours and again for 6.5 hours at 1900°C under helium to obtain additional information concerning the closing of the miscibility gap. Samples from the monocarbide region were also quenched into the liquid tin bath. Powder diffraction X-ray analysis was performed on all samples prepared.

c. The Zr-Hf-C System

The samples for solid-state and some DTA investigations were prepared in the same manner explained in the Ti-Zr-C section above. Most of the melting point samples in the ternary Zr-Hf-C system were prepared by hot pressing the elemental, hydride, and prepared monocarbide powders in graphite dies. Those samples which were quite metal-rich were cold pressed and given a strengthening heat treatment for 1 hr at 1200°C under a vacuum of 5×10^{-5} Torr prior to the actual melting point determinations.

Many samples, especially the metal rich ones, serving as DTA specimens, were cold pressed and arc-melted under helium to provide adequate homogenization without the chance of oxygen and nitrogen contamination.

Samples for metallographic examinations were obtained from arc melted, DTA, and melting point specimens. Furnace quenching was done from pre-determined temperatures on melting point as well as DTA specimens.

3. Melting Points

The melting points of the alloys in the Zr-Hf-C ternary system were determined using the previously described[49] Pirani melting point technique. The melting point furnace was operated under about 2 1/4 atmospheres helium overpressure to minimize metal and carbon losses at high melting temperatures. The temperature measurements were carried out with a disappearing-filament type micropyrometer which was calibrated against a certified, standard lamp from the National Bureau of Standards. The temperature correction for absorbtion in the quartz furnace window, as well as that correction for deviation due to non-black body conditions, have been amply described and validated in a previous report[49]. The melting points of forty-four selected alloys in the Zr-Hf-C ternary were determined using the Pirani technique; many of these samples were subsequently mounted and studied metallographically. All of the samples were further investigated by studying their X-ray diffraction patterns; some of the specimens were analyzed for their carbon content. In no case did the samples lose more than 1-3 atomic percent carbon based on the nominal compositions.

4. Differential Thermal Analysis

The techniques, equipment, and instrumentation used for high temperature differential thermal analysis have been described at length in previous publications[49, 50].

Fifteen DTA samples (Figure 32) were investigated in the Zr-Hf-C system. They were primarily used to confirm incipient melting points determined by the Pirani melting point method. The binary Hf-C and Zr-C systems have very large two-phase areas between the monocarbide solidus and liquidus boundaries; since very little liquid is formed at incipient melting, except in the immediate area of the eutectic or peritectic points, the Pirani methods yields melting points in excess of the true values. This effect is transported into the ternary Zr-Hf-C system in the areas between about 5 to 40 and 48 to 60 atomic percent carbon; however, the difficulty was overcome with the use of the DTA technique, for the formation of the slightest amount of liquid is readily detected by the DTA method.

5. Metallography

Fifty-six samples, which had been either arc melted, or melted in the melting point or DTA furnace were metallographically examined. The melted portions were mounted in an electrically conductive mixture of diallylphtalate-lucite-copper mounting material. Coarse grinding and rough polishing were done on varying grit sizes (120-500) of silicon carbide paper. A fine, highly polished sample surface was ultimately obtained using a suspension of 0.05 micrometer alumina in Murakami's solution on microcloth. Etching solutions and techniques varied greatly with the carbon content of the ternary alloys. It was found that samples in the metal-rich region were best etched using one of the two solutions. A 10% aqueous

oxalic acid mixture developed the microstructure associated with the Zr-Hf α-β transformation, while an aqueous-aqua regia-hydrofluoric acid combination (9 parts H_2O with 1 part of 60% HCl-20% HNO_3-20% HF concentrated acid mixture) increased the contrast between carbide and metal phases. A concentrated solution of the above acid mixture was used to bring out the grain boundaries of single phase monocarbide alloys.

6. X-Ray Analysis

Using the Debye-Scherrer powder X-ray technique, powder diffraction patterns were made of almost all samples post-experimentally using CuK_α radiation. The crystal structures present in the three systems investigated are simple and well known. The IVa metals, titanium, zirconium, and hafnium, undergo a rapid martensitic-like change in the allotropic transformation from the high temperature body-centered cubic structure to the hexagonal-close packed structure. The diffraction lines of the high temperature form were never observed even in rapidly quenched samples. Many of the powdered specimens were stress annealed, prior to X-ray exposure, to provide sharp, clean films for lattice parameter measurements.

To eliminate the film-blackening caused by titanium flourescence radiation, induced by the CuK_α in those samples containing large amounts of titanium; a cover film, which absorbed this soft white radiation was used over the film during the exposure.

7. Chemical Analysis

Carbon analyses were performed using the standard direct combustion method, and either trapping the evolved CO_2 on NaOH and computing carbon content by weight gained, or by measuring the thermal conductivity of the combusted CO_2-O_2 gas mixture.

Some oxygen, nitrogen, and hydrogen analyses were carried out using the vacuum fusion technique in a platinum bath. In general, the interstitial contents reported by the Aerojet Metals and Plastics Chemical Testing Laboratory tended to be somewhat higher than those values reported by the producer. This discrepancy is perhaps explained by the fact that the materials, in their fine powder form, had sufficient time to absorb both additional water vapor and air in the time interval between the supplier's analysis and the quality control analysis at Aerojet.

Far more important, however, were the semi-quantitative spectrographic analyses performed to check on metallic impurities. Excessive amounts of these impurities could easily lead to false phase equilibria and homogeneous ranges in the investigated systems. Furthermore, metallic impurities, if present in excessive quantities, would critically change the melting points of the investigated Zr-Hf-C alloys. The spectrographic analyses showed no great contamination of any one particular element, and in general, the overall sum of metallic impurities was reasonably low, and was well within tolerable limits.

B. EXPERIMENTAL RESULTS

1. The Titanium-Zirconium-Carbon System

Investigations in the system Ti-Zr-C were restricted to the determination of the solid-state phase equilibria at 1500°C, but DTA and quenching experiments were also performed to determine the critical temperature (T_c) of the miscibility gap that exists between the binary monocarbide phases at low temperatures.

Forty-five alloys were equilibrated at 1500°C under a protective, high-purity helium atmosphere; Figure 9 shows the location and qualitative X-ray analysis of these samples.

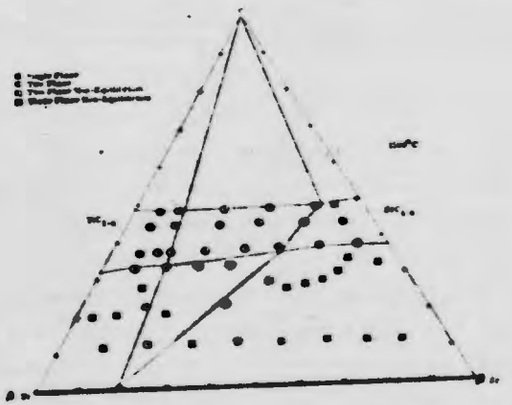

Figure 9. Ti-Zr-C: Location and Qualitative X-Ray Analysis of Samples at 1500°C

A fairly broad miscibility gap was found to exist between the monocarbide phases at 1500°C. The solubility of TiC_{1-x} in ZrC_{1-x} is greater than that of ZrC_{1-x} in TiC_{1-x} (40 Mol % TiC_{1-x} in ZrC_{1-x} as compared to 21 Mol % ZrC_{1-x} in TiC_{1-x}). As might be expected, the immiscibility of the two phases becomes greater with increasing carbon content; in the carbon defect structure, the filled carbon sites afford the cell somewhat less flexibility. Lattice parameter plots of the monocarbide phases between 37.5 and 48 At.% carbon are given in Figures 10-12.

The closing of the miscibility gap between the monocarbide phases was investigated by differential thermal analytical methods as well as by rapid quenching (in tin) techniques (Figure 13). The results

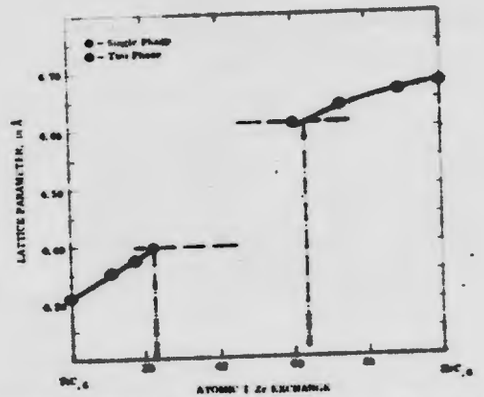

Figure 10. Ti-Zr-C: Lattice Parameters of Monocarbide Solid Solutions at 37.5 At.% Carbon

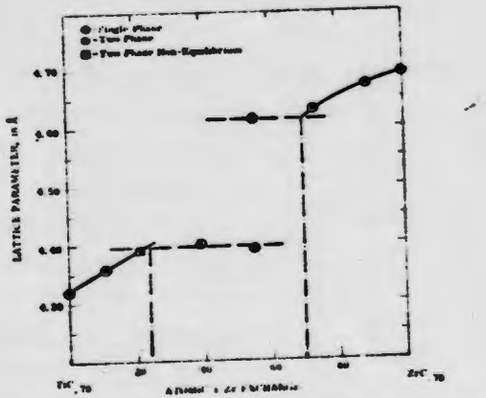

Figure 11. Ti-Zr-C: Lattice Parameters of Monocarbide Solid Solutions at 44 At.% Carbon

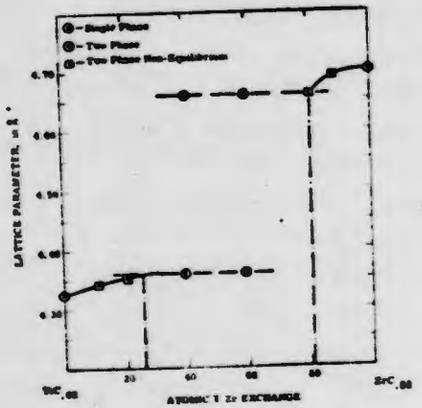

Figure 12. Ti-Zr-C: Lattice Parameters of Monocarbide Solid Solution at 48 At.% Carbon.

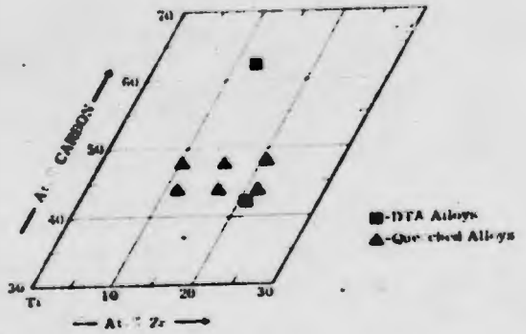

Figure 13. Ti-Zr-C: Location of DTA and Quenching Samples.

in both cases were similar; they indicated the miscibility gap to close on the titanium-rich side of the ternary system and initially at substoichiometric compositions. Figure 14 gives a differential thermogram of an alloy at 42 At.% carbon showing the disproportion of the monocarbide phase upon cooling (~2000°C): the dissolution reaction is found to be initiated at a somewhat higher temperature (~2150°C) in an alloy located in the carbon-rich portion of the diagram (Figure 15). Quenching experiments performed between 1750°C and 2100°C with alloys at 43 and 50 At.% carbon showed the critical composition to be near 50 At.% C at a composition between 15 and 20 Mol. % $ZrC_{\sim 1}$.

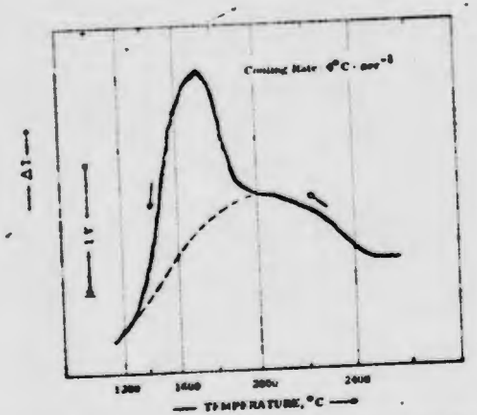

Figure 14. Ti-Zr-C: DTA Cooling Curve of a Ti-Zr-C 21/37/42 Alloy.

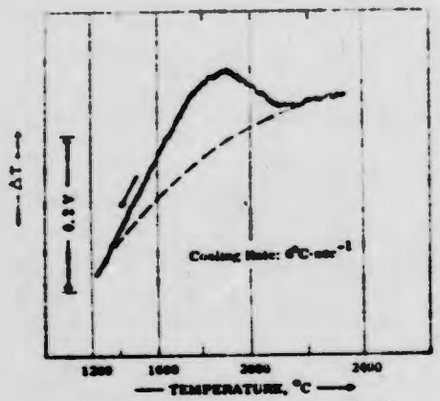

Figure 15. Ti-Zr-C: DTA Cooling Curve of a Ti-Zr-C 13/25/62 Alloy.

The presence of the miscibility gap in the monocarbide region creates two three-phase fields, i.e., TiC_{1-x} (δ) + ZrC_{1-x} (δ') + (Ti, Zr) (β) and TiC(δ) + ZrC (δ') + C. The tie-lines in the metal-rich area between the metal and monocarbide phase were determined from lattice parameter measurements of the respective phases. Figure 16 shows the experimentally determined 1500°C isothermal section.

2. The Titanium-Hafnium-Carbon System

Solid-state investigations were performed, and an isothermal section at 1500°C was established; Figure 17 gives the location and qualitative X-ray analysis of the alloys equilibrated at this temperature.

At this temperature two three-phase fields exist in the ternary; the first, α + β + δ, results from the α-β-transformation of the

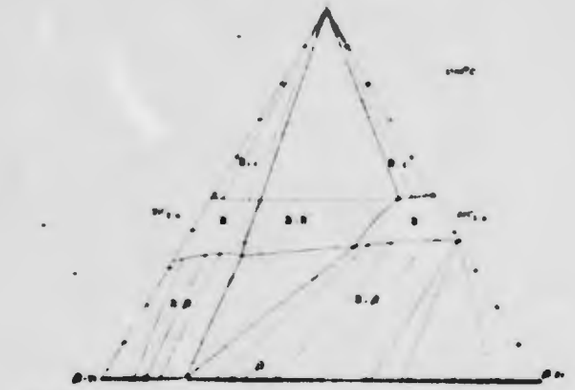

Figure 16. Ti-Zr-C: Section at 1500°C.

Figure 17. Ti-Hf-C: Location and Qualitative X-Ray Analysis of Samples at 1500°C.

of the binary metal solution; the second, $\delta + \delta' + C$, results from the partial miscibility gap existing in the monocarbide solid-solution at high carbon concentrations. With the cooling rates obtainable in the high temperature heat-treating furnace, the high temperature β-form of the metal phase could not be quenched in, and in some cases disproportionation of the monocarbide phase caused the X-ray diffraction patterns to be somewhat diffuse in the back reflection region.

In the metal-rich region of the ternary diagram, the tie-lines were established from lattice parameters; since the β-phase was never retained, measurements could only be made from the low temperature α-form. The three-phase region, $\alpha + \beta + \delta$, was estimated with the aid of the binary metal system[24]; due to the extreme narrowness of this field, it was not confirmed experimentally.

The monocarbide phase was found to form a continuous solid solution only in the extreme carbon defect lattice; with increasing carbon concentration, a miscibility gap exists between the two binary monocarbides.

The closing of the miscibility gap was investigated by differential thermal analytical methods as well as with rapid quenching methods (Figure 18).

The disproportionation of the solid solution was found to start at approximately 2050°C (Figure 22) at the carbon-rich boundary at a hafnium concentration of 12 to 15 At.%. Alloys quenched from between 1800° and 2100°C into liquid tin gave the same results showing that the gap first closes at lower carbon concentrations. Lattice parameters of the TiC_{1-x}-HfC_{1-x} phases are shown in Figures 19-21. Figure 22 shows the

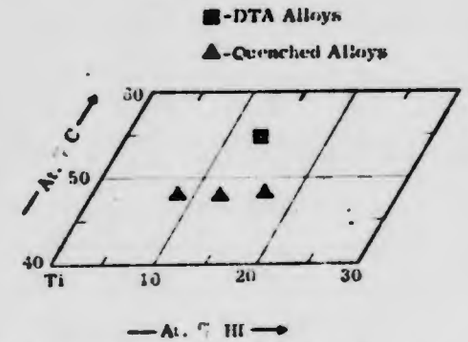

Figure 18. Ti-Hf-C: Location of DTA and Quenching Samples.

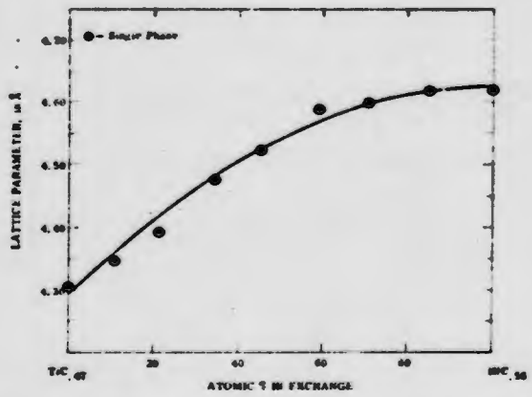

Figure 19. Ti-Hf-C: Lattice Parameters of Monocarbide Phase at 32-36 At.% Carbon 1500°C.

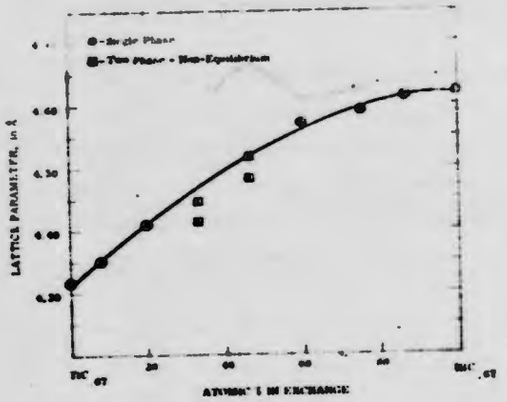

Figure 20. Ti-Hf-C: Lattice Parameters of Monocarbide Phase at 40 At.% Carbon 1500°C.

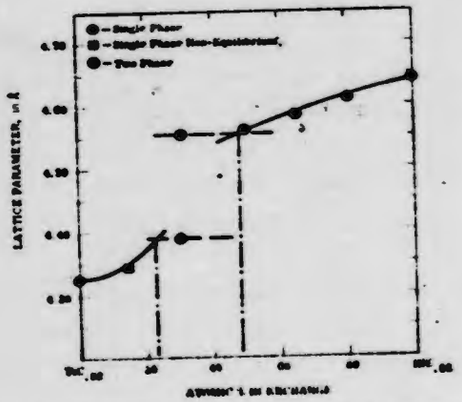

Figure 21. Ti-Hf-C: Lattice Parameters of Monocarbide Phases at 48 At.% Carbon 1500°C.

DTA cooling curves of a Ti-Zr-C 32/13/55 alloy which indicates that disproportionation occurs at about 2050°C. Figure 23 shows the experimentally established isothermal section at 1500°C. At 48 At.% carbon the immiscibility region exists between the TiC_{1-x} (δ) phase with 21 At.% hafnium exchange and the HfC_{1-x} (δ') phase with 50 At.% titanium exchange.

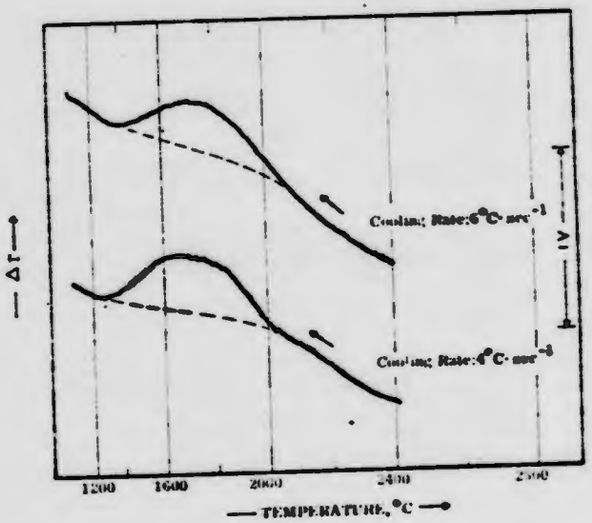

Figure 22. Ti-Hf-C: DTA Cooling Curves of a Ti-Hf-C 32/13/55 Alloy.

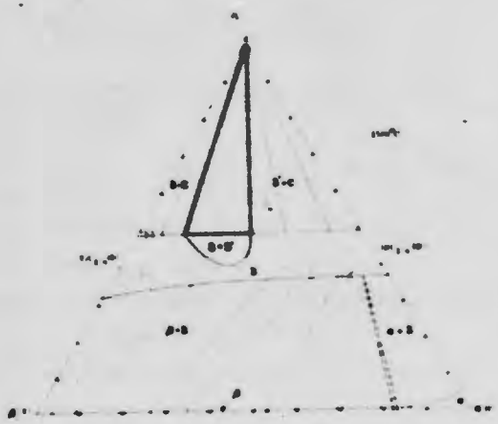

Figure 23. Ti-Hf-C. Section at 1500°C.

3. The Zr-Hf-C System

Thirty-four ternary samples, whose compositional locations are shown in Figure 24, were prepared by hot pressing and heat treating at 1600°C. The locations of the samples have the slight deviations from the nominal compositions (shown by post-experimental analysis) taken into consideration. The following Figure, 25, portrays the qualitative X-ray analysis and phase equilibria at 1600°C.

The films of all the samples which are designated as two-phase showed the monocarbide, B-1 structure, and the low temperature hexagonal close packed α-form of the metal phase. However, strictly speaking, this true equilibria exists only in the extreme hafnium-rich portion of the ternary system where at 1600°C the hafnium-based solid solution still exists in the low temperature form. The zirconium side of the

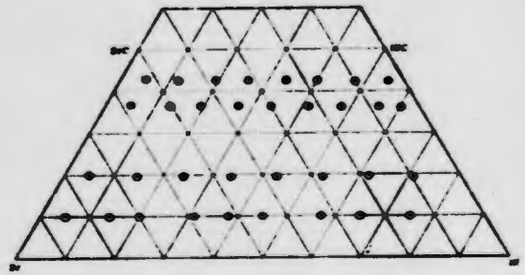

Figure 24. Zr-Hf-C: Location of Solid State Samples at 1600°C.

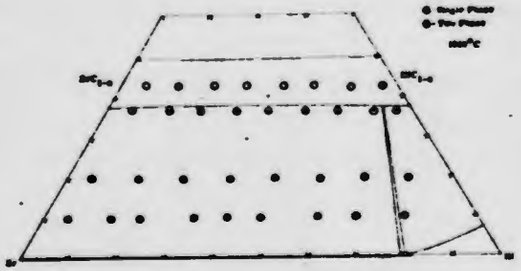

Figure 25. Zr-Hf-C: Qualitative X-Ray Analysis of Samples at 1600°C.

diagram, where the α-β-transformation in the metal phase lies below 1600°, is also two-phase, but the β-form of the metal phase normally present at temperatures above the α-β-transition is completely transformed to the low temperature form on cooling. The binary Zr-Hf system was not specifically investigated in these studies; the variance of the α-β-transformation temperature with composition has been taken from the recent investigations of Thomas and Hayes[24]. Pertinent binary data of the Zr-C[1] and Hf-C[2] systems have been taken from the recent investigations of these systems in this laboratory.

At 1600°C the ZrC_{1-x} and $(Hf_{.94}Zr_{.06})C_{1-x}$ form a complete series of solid solutions. The carbon solubility in the metal solid solution on the zirconium side is quite small, less than 1 At.% C; on the other hand, the low temperature hafnium-richer α-phase dissolves about 7 At.% C at the Hf-C binary. The monocarbide-metal region is divided by a very narrow three-phase β-(Zr,Hf)-α-(Hf, Zr)-(Hf, Zr)C_{1-x} region. Figures 26 and 27 confirm the monocarbide solid solution and depict the measured monocarbide lattice parameters of both single phase (at 43-42.5 At.% C) and slightly two-phase (at 37-36.5 At.% C) alloys as a function of metal concentration. The plot at 43-42.5 At.% C shows a slight negative deviation from Vegard's law. The lattice parameters of the monocarbide phase, taken from two-phase alloys in the $(Zr,Hf)C_{1-x}$-(Zr,Hf) region were used to determine the tie-lines in this two-phase area; the tie-lines are directed toward hafnium-richer monocarbide mixed crystals. Figure 28 shows the lattice parameters and tie-lines of this two-phase region.

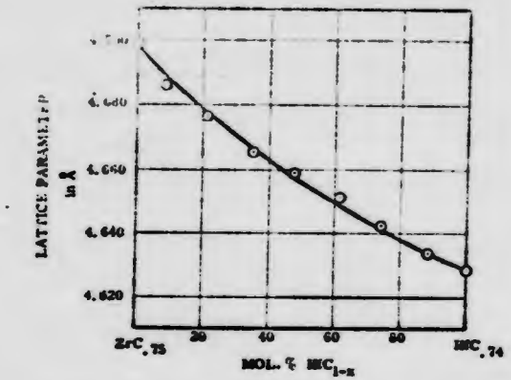

Figure 26. Zr-Hf-C: Lattice Parameters of $(Zr,Hf)C_{.76-.75}$

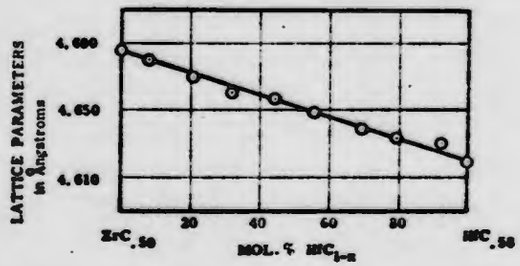

Figure 27. Zr-Hf-C: Lattice Parameters of $(Zr,Hf)C_{.50-.49}$

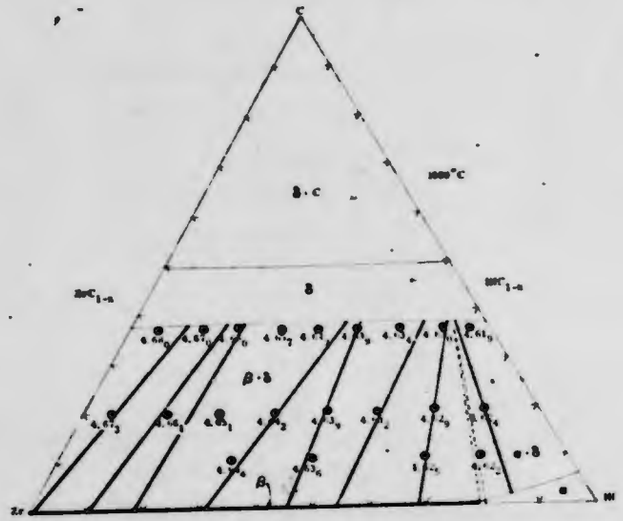

Figure 28. Zr-Hf-C: Monocarbide Lattice Parameters in Ångstroms and Tie Lines in the Metal-Monocarbide Region.

Forty-four melting point samples and fifteen DTA specimens served to establish the incipient melting temperatures of the alloys in the ternary Zr-Hf-C system (Figures 31 and 32).

A eutectic trough, which lies very close to the Zr-Hf binary side, runs across the lower portion of the ternary metal-rich region connecting the binary β-Zr-ZrC_{1-x} and β-Hf-α-Hf(C) eutectica which lie at about 1.5 At.% C in the respective carbide binaries.

Figures 29 and 58 show the location of the eutectic trough as well as the melting-point-tie-line-corrected melting temperatures of the metal-rich ternary eutectic trough. The melting temperatures of the eutectic trough increase smoothly from 1835°C on the zirconium side to 2180°C on the hafnium side.

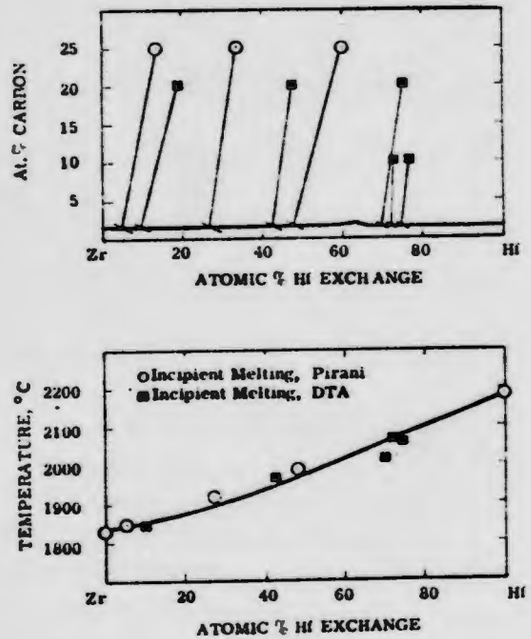

Figure 29. Zr-Hf-C: Tie-Line-Corrected Melting Points and Position of Metal-Rich Eutectic Trough.

The incipient melting points of alloys in the region between 5 and 20 At.% C correspond to the melting points along the metal-rich eutectic trough. By establishing tie lines connecting the respective incipient melting points of the alloys in this region, it was possible to present a melting curve of the eutectic trough although none of the alloys chosen lie directly on the trough itself. Due to the large temperature difference between the solidus and liquidus curves in the region between the metal-rich eutectic and the monocarbide, the alloys melt quite heterogeneously, for very little liquid is formed at the incipient melting points. For alloys in this region, the highly sensitive DTA technique was used to check and confirm melting points obtained with the Pirani hole method.

Extensive metallography of melting point, arc melted, and DTA samples (location of samples in Figures 30, 31, and 32) as well as comparison of ternary eutectic trough melting points with those of the Hf-Zr binary aided in locating the metal-rich eutectic trough.

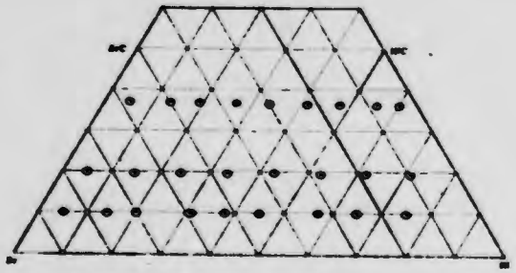

Figure 30. Zr-Hf-C: Location of Arc Melted Samples

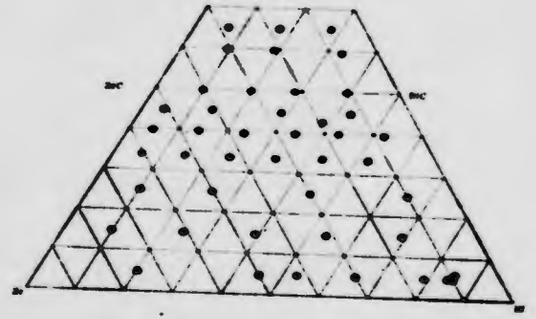

Figure 31. Zr-Hf-C: Location of Melting Point Samples.

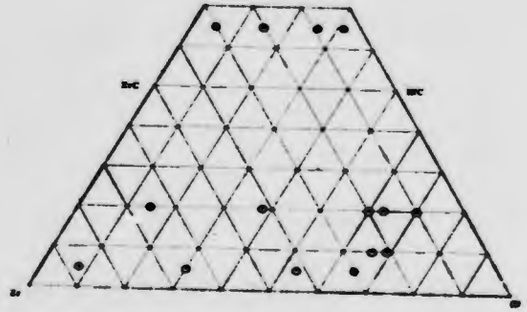

Figure 32. Zr-Hf-C: Location of DTA Samples.

It was difficult to obtain pictures of a eutectic in this region; the reason for this is that the eutectic lies very close to the metal binary and contains but a very small amount of carbide phase. Alloys with 5 atomic percent carbon and less on the zirconium side showed considerable amounts of primary carbide indicating the eutectic to lie quite close to the metal binary. The metal phase present in the metal-rich region showed an unusual microstructure which is attributed to the α-β-transformation transition on cooling. All evidence of this transformation vanished when the quenched samples were subsequently heat treated below the transformation temperature. Figures 33 to 37 show the metallographic findings in the zirconium metal-rich portion of the ternary Zr-Hf-C system.

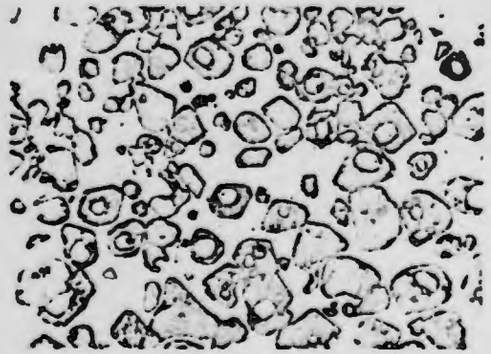

Figure 33. Zr-Hf-C: 75/10/15, Quenched from Approximately 1900°C. X1000

Primary Monocarbide (Dark) in Metal Matrix (Light). Metal α-β-Transformation Not Resolved.

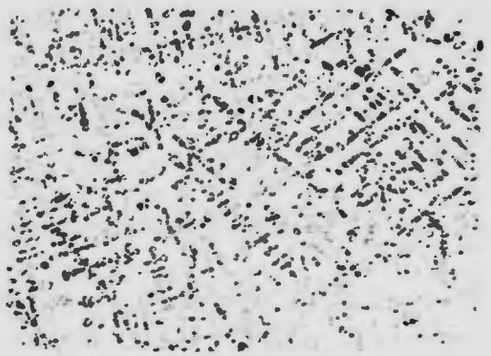

Figure 34. Zr-Hf-C: 59 31 10, Arc Melted X240

Primary Monocarbide Dendrites (Grey) in Metal Matrix (Light)

Metal Transformation in Metal Matrix not Completely Resolved.

Figure 35. Zr-Hf-C: 65/30/5, Arc Melted X240

Primary Monocarbide (Light) in Metal Matrix (Grey) α-β Metal Transformation in Metal Matrix.

Figure 36. Zr-Hf-C: 45/45/10, Arc Melted. X600
Primary Monocarbide (White) in Metal Matrix (Grey)
α-β Metal Transformation (Ripples) in Metal Matrix.

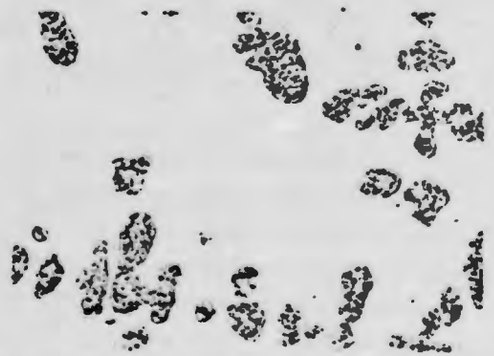

Figure 37. Zr-Hf-C: 45/45/10, Arc Melted + 4 hrs./1200°C X1000
Primary Monocarbide (Dark) in α-Metal Matrix (Light).
α-β Transformation Vanished.

The α-metal phase, which is stabilized to higher temperatures in the Hf-C binary[2], and projects itself into the ternary field in the temperature range of 1900° to 2360°C as well as partaking in a four-phase reaction at 2030°C, was the object of extensive metallographic and DTA studies to determine its homogeneous range.

DTA samples, located at 20 At.% carbon on the hafnium-rich side of the ternary, traced the incipient melting points of the peritectic decomposition of the α-phase as a function of zirconium content. The incipient melting points enable the zirconium solubility limits of the α-phase to be determined at the respective melting temperatures. The maximum solubility of zirconium in the close-packed hexagonal phase was found to be at 25 At.% Zr exchange; the incipient melting temperatures of alloys beyond this point toward the zirconium-richer side remained constant in the small four-phase region. Figures 38 and 39 depict the incipient melting temperatures (maximum solubility for Zr) of the α-phase as well as the four-phase reaction plane temperature.

With increasing temperature, the metal-rich eutectic-trough liquid advances along the metal-rich portion of the ternary region. At 2030°C a four-phase Class II reaction:

$$\beta\text{-(Hr, Zr)} + (Hf, Zr)C_{1-x} \underset{(T = 2030°)}{\overset{T > 2030°}{\rightleftharpoons}} \text{Liquid} + \alpha\text{-Hf(C, Zr)} \text{ occurs.}$$

The four-phase reaction plane is quite small and is shown in Figures 55 and 62.

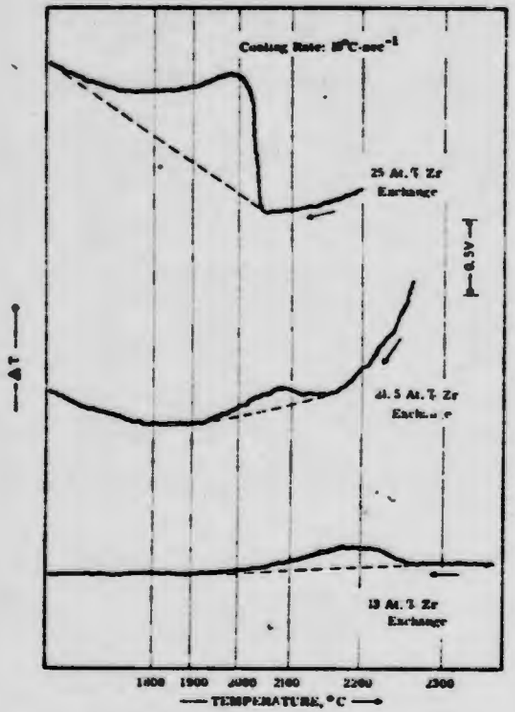

Figure 38. Zr-Hf-C: Differential Cooling Curves at 20 At.% Carbon with 13-25 At.% Zirconium Exchange.

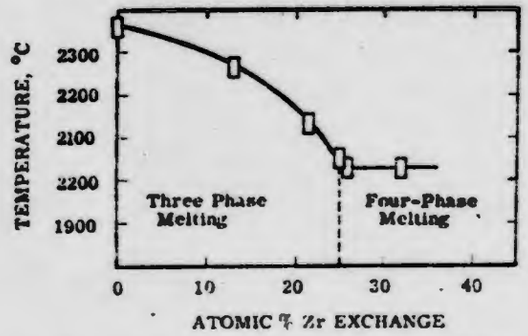

Figure 39. Zr-Hf-C: Incipient Melting (Maximum Solidus) of α-Phase; Four-Phase Plane Reaction Temperature.

After the eutectic trough passes under the extended, stabilized α-phase, the α-phase slowly retracts toward the Hf-C binary with increasing temperature and disappears at 2360°C, the peritectic temperature in the Hf-C binary.

The solubility limits of the α-phase, both for zirconium and carbon were determined metallographically to confirm the findings of the DTA experiments. In this manner the domain of the four-phase plane as well as the homogeneous region of the α-phase were established. The α-phase was relatively easily detected and differentiated from the high temperature β-form of the metal solid solution by virtue of the fact that the α-phase almost always showed heavy, oriented carbide precipitates in the individual grains and, furthermore, did not have evidence of the α-β transformation. The β-phase, on the other hand, had almost no carbide

precipitates, indicating a very small carbon solubility at the most, in many cases the microstructure of the β-phase showed the characteristic ripples of the α-β metal transformation on cooling.

The high temperature stabilized α-phase, was not detected metallographically in alloys whose zirconium content was greater than 35 At.% Zr (Figures 55 and 62). Since the liquid phase on the eutectic trough was found to have advanced very close to the composition Zr-Hf-C 35/63.5 1.5 at the four-phase plane reaction temperature 2030° (Figure 62), the agreement of metallographic findings with those determined by melting temperatures in locating the four-phase region are deemed to be in excellent accord. Metallographic pictures of some of the many alloys prepared and investigated in the hafnium-rich corner of the ternary are presented in Figures 40 to 45.

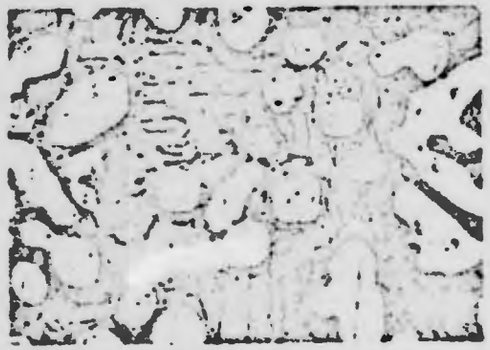

Figure 40. Zr-Hf-C: 35/45/20, Quenched from 3100°C. X700

Primary Monocarbide (White) in Metal Matrix (Dark) Showing α-β Transformation (Black).

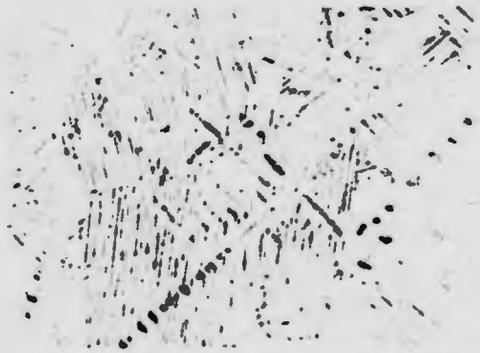

Figure 41. Zr-Hf-C: 15/75/10, Quenched from 2950°C. X375

Primary Monocarbide Dendrites (Grey) in α-Hf Matrix With Heavy, Oriented Carbide Precipitates (Black).

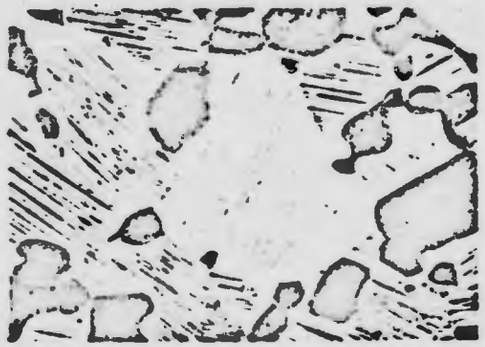

Figure 42. Zr-Hf-C: 11/79/10, Equilibrated at and Quenched from 2250°C - Above Peritectic Temperature. X500

Monocarbide (Black) in α-Hf Metal Matrix with Heavy, Oriented Carbide Precipitates.

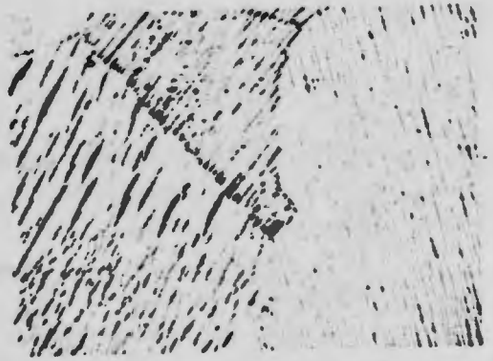

Figure 43. Zr-Hf-C: 11/79/10, Quenched from 2100°C. X400
Below Peritectic Temperature α-Hf(Zr,C) With Oriented Carbide Precipitates.

Figure 44: Zr-Hf-C: 30/65/5, Quenched from Approximately 2000°C. X600
α-Hf(Zr,C) (Light Grey) Showing Oriented Carbide Precipitates (Dark Grey Streaks) and Primary Carbide (White) in an α-Zr,Hf Metal Matrix (Dark Grey) Showing α-β Transformation (Dark Black Ripples with Shiny Gaps).

Figure 45. Zr-Hf-C: 16 79/5, Quenched from 2100°C - X1000
Polarized Light.
Single Phase α-Hf(Zr,C).

Metallographic and X-ray results of samples quenched from 2500 - 2800°C show that the metal-rich boundary of the monocarbide solid-solution does not differ to any great degree from its location at lower temperatures across the greater portion of the ternary diagram in this temperature range. At higher temperatures, the lower (metal-rich) boundary of the ternary monocarbide phase recedes toward higher carbon concentrations just as it does in the respective binaries. No metal precipitates could be observed in the carbide grains. The lower metal-rich boundary of the monocarbide phase in the Hf-C binary increases its limits (compared to higher temperatures) to slightly lower carbon concentrations at the peritectic temperature of 2360°C; this, however, is not the case in the Zr-C binary where the lower boundary of the monocarbide homogeneous range remains constant at temperatures below about 2800°C.

Figures 46, 47, and 48 depict the typical fissuring along the metal-carbide boundary of the monocarbide region. These results are also incorporated in the series of isothermal sections shown in Figures 59 to 67.

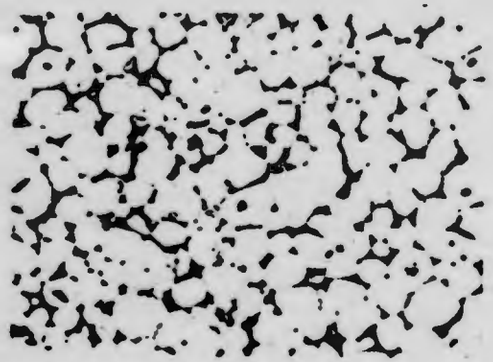

Figure 46. Zr-Hf-C: 41/25/34, Quenched from Approximately 2500°C. X600

Monocarbide Grains (White) with Small Amounts of Metal Phase (Black) in Between Grains.

The binary monocarbides in HfC_{1-x} and ZrC_{1-x} both exhibit a considerable homogeneous range from 49.5 At% to about 37.5 At.% carbon at 1600°C. In the ternary, the carbides form a complete series of solid solutions.

The melting points, as determined on several alloys (Figure 31) in the monocarbide region at 45 At.% and 47.5 - 49.5 At.% C, show that there are no maxima or minima in the solidus curves. The

Figure 47. Zr-Hf-C: 11/55/34, Quenched from 3400°C. X1000

Monocarbide Grains (Grey) with Small Amounts of Metal Phase (Mottled White) in Between Grains.

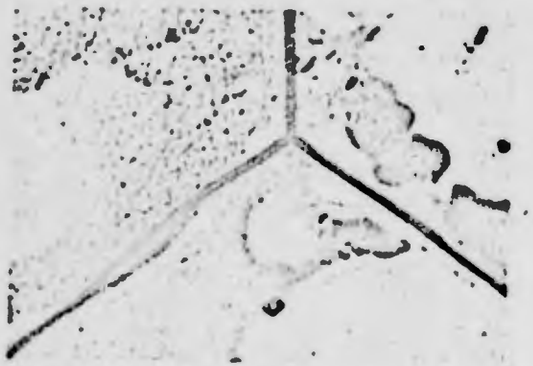

Figure 48. Zr-Hf-C: 25/35/40, Enlarged Approximately Twice for Reproduction. Quenched from 3500°C. X1000

Single-Phase Monocarbide with Slight Coring in Grains.

maximum solidus curve of the monocarbide solid solution runs smoothly from 48.5 At.% C on the hafnium side to 45 At.% C on the zirconium side; the melting points decrease smoothly from 3928°C at $HfC_{.94}$ to 3440°C at $ZrC_{.82}$.

Alloys in this region, which did not lie on the maximum solidus line between the binary monocarbides, were observed to melt increasingly less sharply with increasing amounts of hafnium; the large temperature difference in the liquidus and solidus lines of the Hf-C binary in the monocarbide region is projected into the ternary. Figures 49 and 50, show the incipient melting points of the alloys in the monocarbide region.

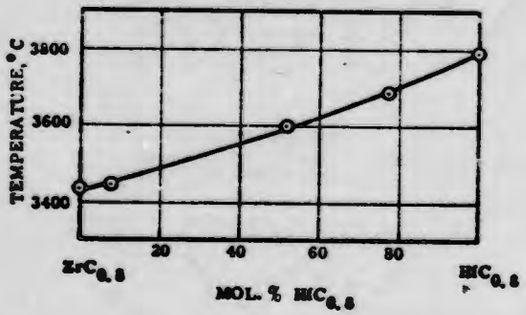

Figure 49. Zr-Hf-C: Melting Points of $(Zr,Hf)C_{.8}$ Alloys

The carbon-rich boundary of the monocarbide region is slightly hypostoichiometric at the binary edges as well as across the ternary. No free carbon analysis were made on solid state samples, but analysis results of free and combined carbon on several melting point

specimens indicated the extention of the rather broad, congruent melting maximum of the $ZrC_{.82}$ into the ternary, and that the carbon-rich boundary decreases in carbon content (with increasing temperature) along a line joining the respective binary monocarbide boundaries.

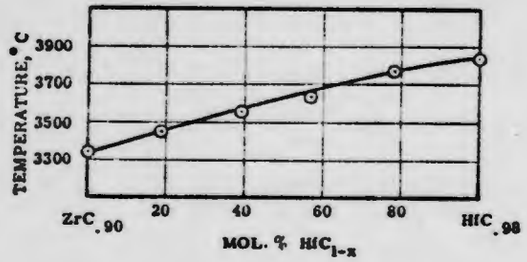

Figure 50. Zr-Hf-C: Melting Points of $(Zr,Hf)C_{.90-.98}$ Alloys

Metallographic evidence and melting point data ascertained that a eutectic trough, which runs almost linearly across the ternary field between the Hf-C binary eutectic at 65 At.% C and the Zr-C binary eutectic at 64.5 At.% C, is present in the region between the monocarbide solid-solution and graphite. The eutectic melting points decrease smoothly from the hafnium side at 3180° to 2911°C on the zirconium side.

Melting point results obtained on alloys in this region using the Pirani-Hole-Method were rather inconsistent due to the extremely heterogeneous melting of the alloys; the DTA technique was used to establish accurate melting points along the carbide-graphite eutectic trough. Figures 51 and 52 portray the metallographic microstructures typical of alloys in this region.

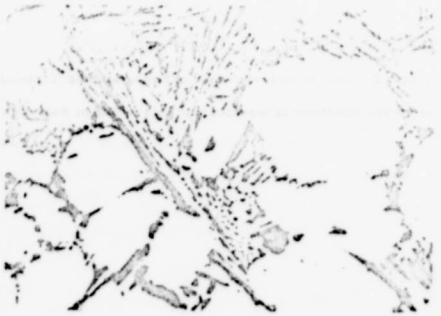

Figure 51. Zr-Hf-C: 30/10/60, Enlarged Approximately X500
Twice for Reproduction. Quenched from 3050°C.
Primary Monocarbide Grains (White) in Graphite-Monocarbide (Partially Garbide Depleted) Eutectic Matrix (Black-White).

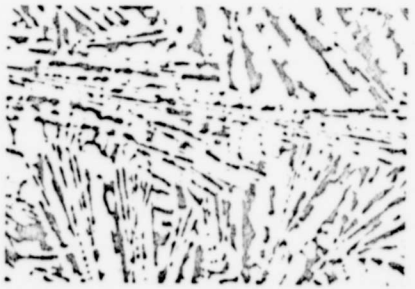

Figure 52. Zr-Hf-C: 28/7/65, Quenched from 2990°C. X1000
Monocarbide-Graphite Eutectic.

A DTA curve, typical of the results on alloys in the monocarbide-graphite region, showing melting and solidification on the eutectic trough is depicted in Figure 53. In Figure 54 the melting points of the

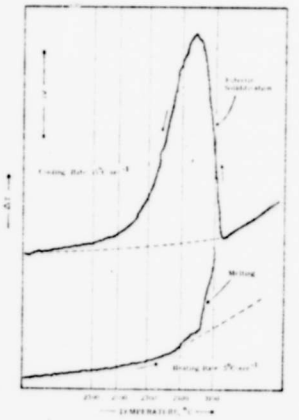

Figure 53. Zr-Hf-C: Differential Heating and Cooling Curves
of an Zr-Hf-C 3.5/31.5/65 Alloy.

ternary carbide-graphite eutectic trough are plotted as a function of composition. The location of the trough is to be seen in Figure 58.

The experimental evidence obtained in all the investigations of the Zr-Hf-C system is compiled in a three-dimensional space-model diagram presented in Figure 55.

Since the reaction rates at lower temperatures are expected to be extremely slow, with the exception of the α-β metal transformation, which was not investigated in detail, no experimental investigations were carried out below 1600°C.

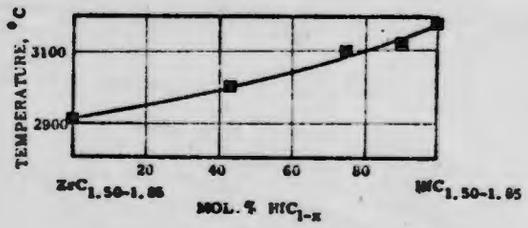

Figure 54. Zr-Hf-C: Melting Points of Monocarbide-Graphite Eutectic Trough.

A series of temperature sections from 1600°C to 3900°C are presented in Figures 59 to 72 to aid in the visualization of the space model.

Small temperature intervals were taken with several adjacent temperature sections in the vicinity of the four-phase reaction plane to depict more clearly the phase equilibria near these temperatures. One isopleth, at 10 At.% carbon (Figure 56), containing the equilibria of the metal-rich portion of the ternary Zr-Hf-C system is also presented; should the need for further isopleths arise, they may be easily developed from the temperature sections.

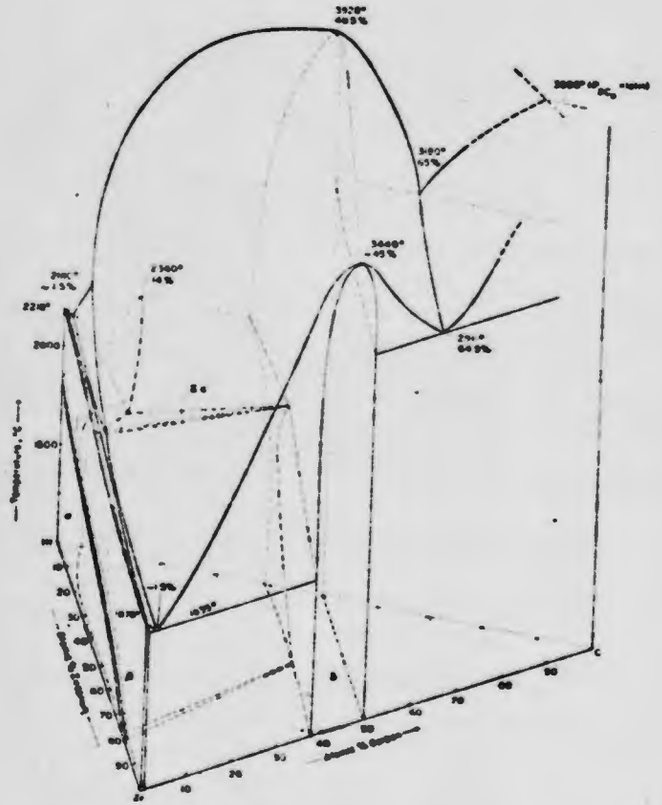

Figure 55. Zr-Hf-C: Three-Dimensional Space-Model.

The invariant and univariant (p = const.) reactions occurring in the ternary Zr-Hf-C system, along with those reactions of the corresponding binary systems, are compiled in a Scheil-Schultz diagram shown in Figure 57. A diagram (Figure 58) showing the maximum liquidus

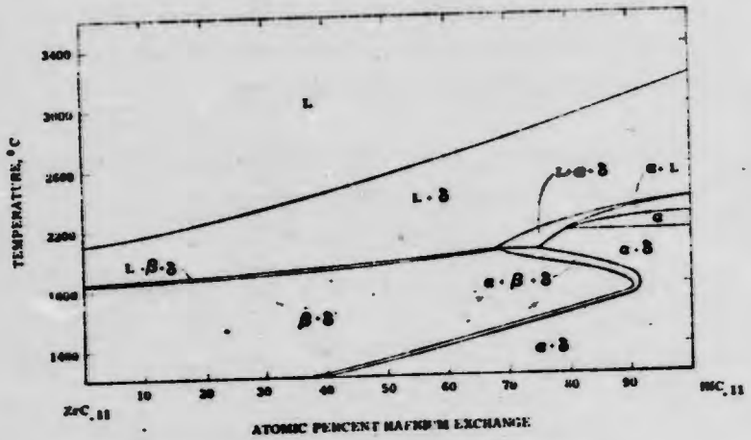

Figure 56. Zr-Hf-C: Isopleth at 10 At.% Carbon.

curves, estimated as closely as possible from melting point data, of the entire Zr-Hf-C system is presented as a final supplement to the phase equilibrium data.

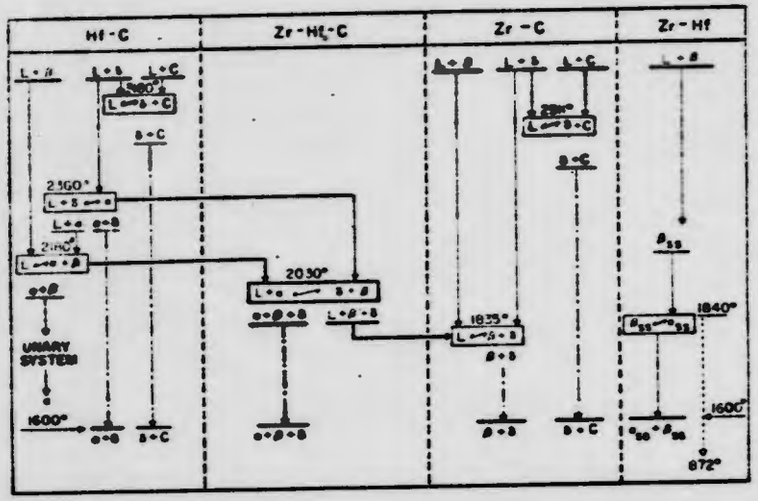

Figure 57. Zr-Hf-C: Scheil-Schultz Diagram.

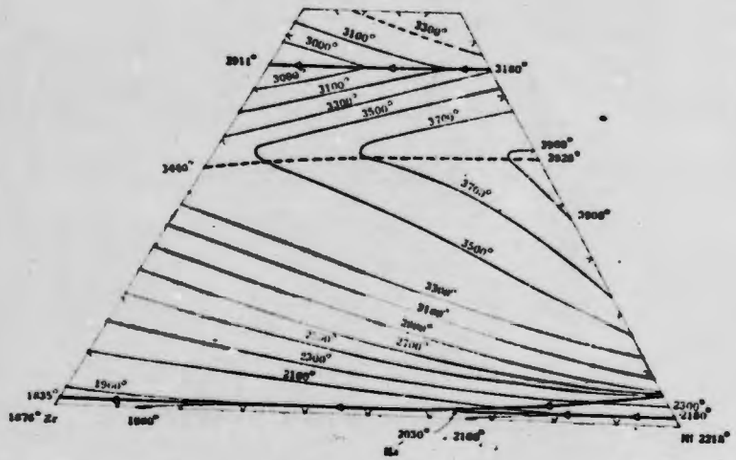

Figure 58. Zr-Hf-C: Liquidus Projection.

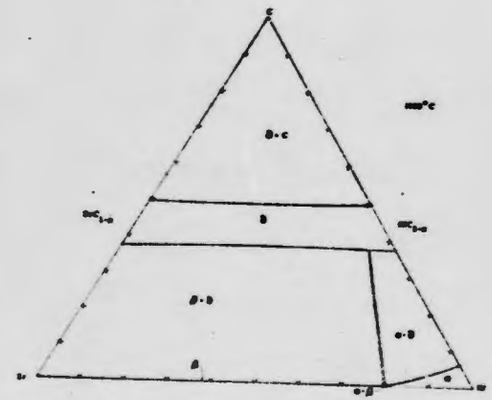

Figure 59. Zr-Hf-C: Section at 1600°C.

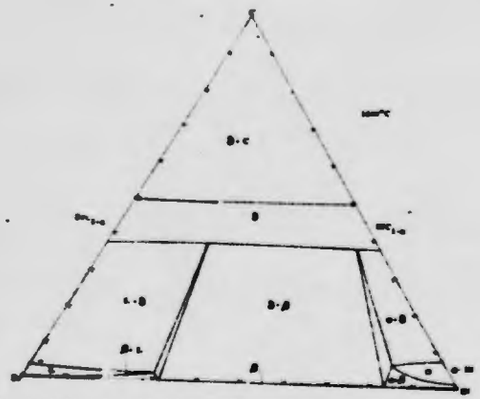

Figure 60. Zr-Hf-C: Section at 1900°C.

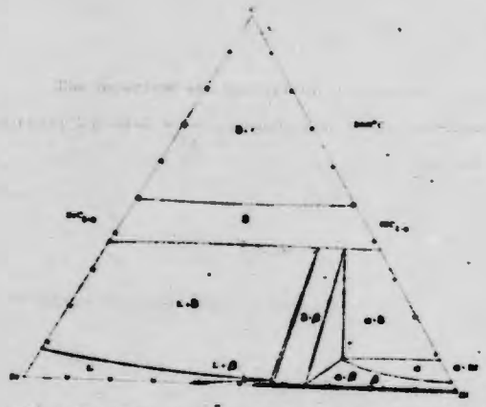

Figure 61. Zr-Hf-C: Section at 2000°C.

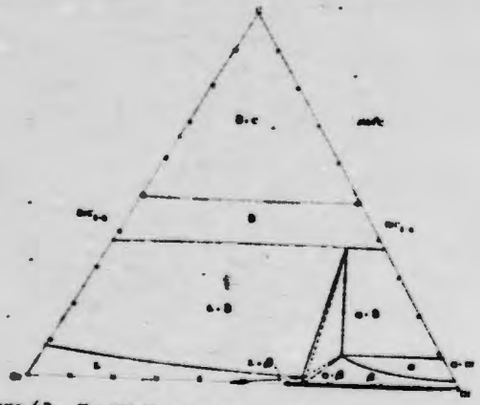

Figure 62. Zr-Hf-C: Section at 2030°C.

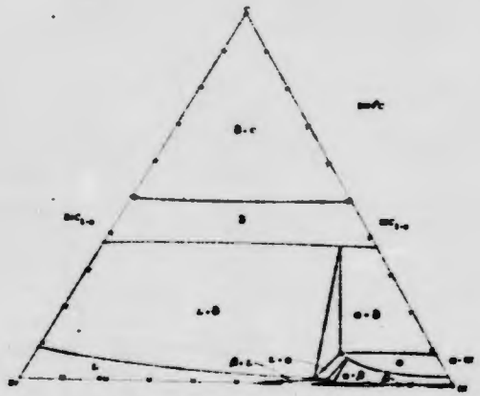

Figure 63. Zr-Hf-C: Section at 2060°C.

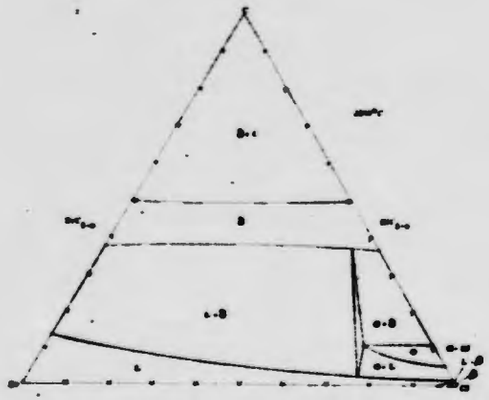

Figure 64. Zr-Hf-C: Section at 2200°C.

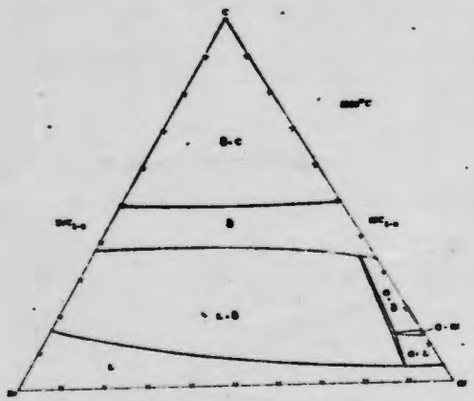

Figure 65. Zr-Hf-C: Section at 2320°C.

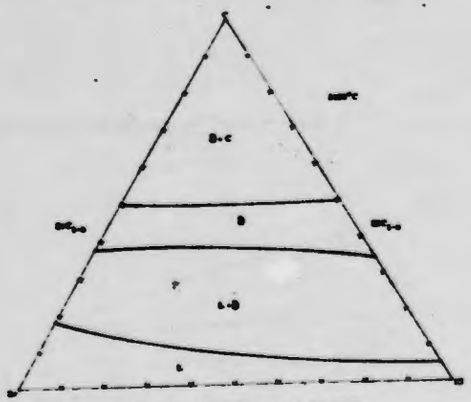

Figure 66. Zr-Hf-C: Section at 2400°C.

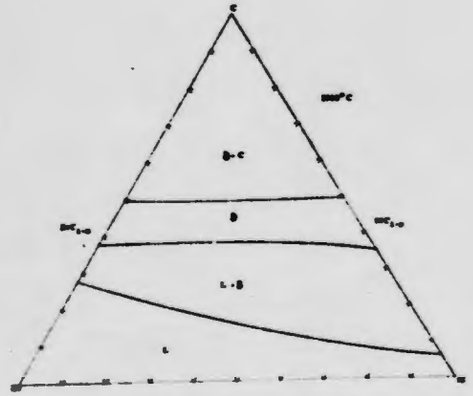

Figure 67. Zr-Hf-C: Section at 2800°C.

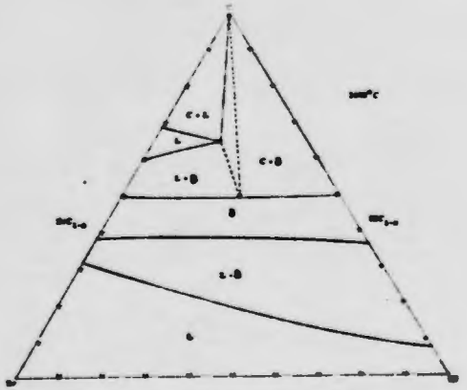

Figure 68. Zr-Hf-C: Section at 3000°C.

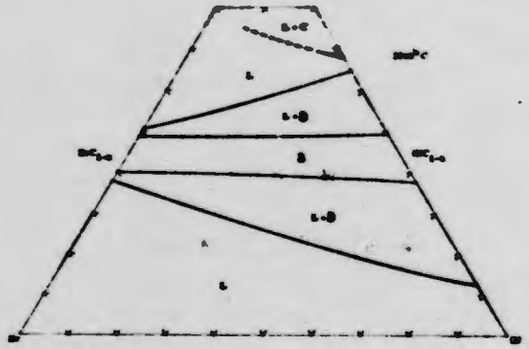

Figure 69. Zr-Hf-C: Section at 3300°C.

Figure 70. Zr-Hf-C: Section at 3500°C.

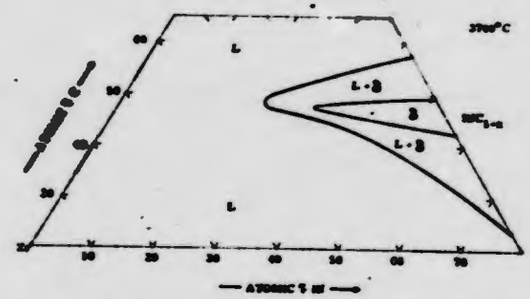

Figure 71. Zr-Hf-C: Section 3700°C.

Figure 72. Zr-Hf-C: Section at 3900°C.

IV. DISCUSSION

A. PHASE EQUILIBRIA

The appearance and shapes of the monocarbide miscibility gaps in the Ti-Zr-C and Ti-Hf-C are an effect of the rather large difference in atomic radii of the Ti-Zr and Ti-Hf pairs. At 1500°C the ZrC_{1-x} and TiC_{1-x} are completely immiscible although HfC_{1-x} and TiC_{1-x} form a complete series of solid-solutions in only the extreme carbon defect lattice; the monocarbide miscibility gap in the Ti-Zr-C system closes completely at a higher temperature than the gap in the Ti-Zr-C system — these data reflect the fact that the atomic radius of hafnium is slightly smaller than that of its sister element zirconium. This observation concerning hafnium and zirconium, as well as their isostructural compounds, has been expressed several times in the past.

An examination of the slopes of the tie lines in the two-phase metal-monocarbide regions of the Ti-Zr-C, Ti-Hf-C, and Zr-Hf-C ternary systems indicate the relative stability of the carbide pairs at the metal-rich carbide boundaries. It is seen that the free energies of formation must become less negative in the progression $HfC_{1-x} > ZrC_{1-x} > TiC_{1-x}$, for the tie lines are always inclined toward that carbide solid-solution richer in the carbide component with the more negative free energy of formation. A cursory calculation of the free energies of formation of these monocarbides at compositions near the metal-rich boundary of the carbide homogeneous ranges (37.5 At.% C for comparison purposes) at 1500°C using the data of Y. A. Chang[51] resulted in the following data (Table 3) for the carbon-defect monocarbides:

Table 3. Calculated Free Energies of Formation of Group IVa Monocarbides.

Carbon-Defect Monocarbide	ΔG_f at 1500°C cal/gram-atom of Metal
$TiC_{.6}$	-15,061
$ZrC_{.6}$	-16,693
$HfC_{.6}$	-18,864

This data is in accord with the stabilities indicated by the slopes of the tie lines (see Figures 16, 23 and 28).

B. APPLICATIONS

Although only solid-state investigations have been carried out in the Ti-Zr-C and Ti-Hf-C systems, predictions of high temperature phase-equilibria and behavior as well as high temperature application possibilities can be made.

In view of the phase equilibria exhibited by the Ti-Zr-C system at 1500°C, coupled with the facts that the miscibility gap in the monocarbide region closes at approximately 2150°C, and the β-Ti-TiC_{1-x} eutectic temperature is rather low (1650°C); high temperature applications of ternary alloys of this system are slightly limited. Only the fact that the α-β transformation temperature is quite low in both titanium and zirconium (870-880°C) prevents the possible use of composite Ti-Zr-C alloys from being almost totally discarded. The two, two-phase regions, (Ti, Zr)-(Ti, Zr)C_{1-x} and (Zr, Ti)-(Zr, Ti)C_{1-x} which lie on either side of the metal-rich, three-phase area provide the necessary phase equilibria for composite refractory metal-carbide bodies. The unrestricted choice of compatible carbide compositions is limited by the presence of the miscibility gap. To avoid

structural failures caused by repetitive solutioning and disproportionationing of the carbide phase during temperature cycling, composite alloys having carbide compositions outside the $(Ti, Zr)C_{1-x}$-$(Zr, Ti)C_{1-x}$-(Ti, Zr) three-phase field must be chosen. That is, a rather titanium-rich $(Ti, Zr)C_{1-x}$ carbide would have to be mated with a titanium-rich (Ti, Zr) metal phase or, a zirconium-rich $(Zr, Ti)C_{1-x}$ carbide would be paired with a zirconium-rich (Zr, Ti) metal phase, whereby the choice in the composition of the metal phase in the latter case is afforded a greater latitude by virtue of the larger existing two-phase region. More detailed investigations would be necessary to determine the critical closing temperature of the metal-rich monocarbide boundary, although the limiting factor in high temperature applications for these alloys is not the closing of the miscibility gap, but rather the appearance of liquid at 1650°C in the Ti-C binary. It is reasonable to assume that melting temperatures of the eutectic trough increase smoothly from 1650°C on the titanium side to 1835°C on the zirconium side. The majority of the ternary defect-monocarbide compositions would already be in equilibrium with eutectic liquid even if the monocarbide miscibility gap would close at a temperature in the vicinity of 1800° or higher. The choice of ternary, composite alloys in the Ti-Zr-C system for high temperature application is limited from 880°C to approximately 1600° - 1750°C, depending on the zirconium content.

Small additions of a third refractory metal, such as niobium or tantalum would lower the critical closing temperature of the monocarbide miscibility gap and even provide somewhat higher melting temperatures along the eutectic trough.

High temperature applications of titanium-zirconium monocarbides in contact with graphite in composite bodies are feasible, but either with only a limited compositional choice at temperatures below about 2150°C, the critical closing temperature of the miscibility gap on the graphite-rich boundary of the monocarbide region, or exclusively in the temperature range of about 2200° to 2700-2900°C (depending on zirconium content), the melting points of the ternary monocarbide-graphite eutectic. Excessive temperature cycling below 2150°C would give rise to solutioning and disproportionationing of the monocarbide phase and lead to structural failure of a proposed work piece.

In contrast to the Ti-Zr-C system, which has a large miscibility gap in the monocarbide region at 1500°C, the monocarbide area in the Ti-Hf-C ternary system displays complete solid-solubility along the metal-rich boundary of the carbide phase. As has been pointed out, in the Ti-Zr-C system however, this fact is not the most critical one for the selection of alloys for high temperature use. The limiting factors for metal-rich composite Ti-Hf-C alloys will be the α-β transformation temperature of the metal phase. This transformation temperature will vary from 880° upwards depending on the hafnium concentration; alloys chosen for high temperature applications would be subject to the effects of this structural change. This particular point is discussed further in subsequent paragraphs.

Again, although only a solid-state section was investigated in this system, predictions concerning high temperature phase equilibria influencing high temperature applications can be made. The α-metal phase will most probably be stabilized into the ternary toward higher carbon concentrations; the solubility of the α-phase for titanium will probably not be as

large as in the Zr-Hf-C system, and the α-phase will most probably partake in a four-phase reaction similar to that in the Zr-Hf-C system. Since the monocarbide miscibility gap closes on the carbon-rich side at about 2050°C, the three phase region (Ti, Hf)C_{1-x}-C-(Hf, Ti)C_{1-x} region will vanish to a limiting tie line. The statements made concerning the application possibilities of composite alloys in carbon-rich region of the Ti-Zr-C system apply here to the Ti-Hf-C system.

High temperature application possibilities of materials whose compositions lie in the metal-rich region will be governed by the extent of the homogeneous range of the α-phase as well as the unfortunately low melting (on the Ti-side) ternary eutectic trough.

In the Zr-Hf-C ternary system, the region of primary interest, the area between the monocarbide and the metal binary phase, shows some promise of providing suitable alloys for high temperature composite materials, although full utilization of the higher melting points on the hafnium-richer side of the ternary diagram will not be able to be realized. The α-Hf phase, which is stabilized to higher temperatures by incorporating carbon atoms into the host metal lattice, shows a strongly temperature dependent solubility for both carbon and zirconium. Proposed composite alloys, whose composition would be in the regions controlled by the α-phase, are subject to the rapid solutioning and disproportionationing reactions of the α-phase and would certainly be of little value for high temperature application in a temperature cycling environment. Since the homogeneous range of the α-phase varies so strongly with temperature between about 1600° and 2000°C, even small temperature changes in a proposed composite alloy in this region would severely hamper effective usage. Zirconium-richer

alloys, lying outside the regions influenced by the stabilized α-phase, are to be considered possible for moderately high temperature applications; a whole series of metal phase compositions in equilibrium with various monocarbides with overall hafnium content not exceeding about 65 At.% exhibit two-phase, monocarbide-metal equilibria. Depending on the hafnium content, the maximum usable temperatures appear to be around 1900°C. The α-β transformation temperature varies from about 870°C, for pure zirconium, upwards with increasing hafnium content in the region of interest. Again, the structural changes caused by heating and cooling composite alloys through this metal-composition-dependent transformation temperature will subject the composite body to mechanical stresses. The ductility of the metal phase itself may, however, overcome this difficulty and permit extensive use of such composite bodies even in a temperature cycling environment.

The use of composite bodies, containing zirconium-hafnium monocarbide and graphite, appears to present no particular difficulties, and proposed high temperature applications would be limited only by the melting points of the monocarbide-graphite eutectic which vary between 2911° and 3180°C, depending on the hafnium concentration.

REFERENCES

1 E. Rudy, D.P. Harmon, and C. E. Brukl, AFML-TR-65-2, Part I, Vol. II (1965).

2 E. Rudy, C. E. Brukl, and D.P. Harmon: AFML-TR-65-2, Part I (1965).

3 G. Hagg: Z. Phys. Chem., 11 (1930) 433.

4 R. B. Russell: J. Appl. Phys., 24 (1953) 232.

5 J. D. Fast, J. Appl. Phys. 23 (1952) 350.

6 W. G. Burgeors and F.M. Jacobs: Z.Krist., A94 (1936) 299.

7 R. B. Russell: J. Metals, 6 (1954) 1045.

8 P. Duwez: J. Appl. Phys., 22 (1951) 1174.

9 W.B. Pearson: "A Handbook of Lattice Spacings and Structures of Metals and Alloys", Pergamon Press, New York (1958).

10 T. H. Schofield and E. A. Bacon: J. Inst. Metals, 82 (1953), 167.

11 J. H. deBoer and J.D. Fast: Z. Anorg. u. Allgem.Chem., 187 (1930) 177.

12 N.A. Lange: "Handbook of Chemistry", Handbook Pub., Co., Sandusky, Ohio (1946).

13 P. Duwez: Trans. AIME, 191 (1951) 765.

14 D.K. Deardorff and E.T. Hayes: Trans AIME, 206 (1956) 509.

15 R.V. Sara: J. Amer. Ceram. Soc., 48 (1965) 243.

16 G. Zeitkher: Physica, 6 (1926), 361.

17 D.K. Deardorff and H. Kato: Trans. AIME, 227 (1963) 264.

18 P.A [illegible]mans, O.G. Paasche, and H. Kato: J.Less-Common Metals, 8 (1965) 213.

19 N. J. Grant and B.C. Giessen, WADD 60-132 (1960).

20 R.G. Rees and W. Hume-Rothery: J.Less-Comm.Metals 5 (1963)258.

REFERENCES (Cont.)

21 R.V. Sara and C.E. Lowell: WADD TDR-60-143, Part V (1964).

22 E.T. Hayes, A.H. Roberson, and O.G. Paasche: U.S.B.M. Rept. of Invest. 4823 (1951).

23 D.J. McPherson and M. Hansen: Z. Metallk., 45 (1945) 76.

24 D.E. Thomas and E.T. Hayes: "The Metallurgy of Hafnium", Supt. of Documents, U.S. Gov.Printing Office, Washington 25, D.C.

25 A.E. Van Arkel: Physica, 4 (1924) 286.

26 P. Ehrlich: Z. Anorg.Chem. 259 (1949) 1.

27 L. Stone and H. Margolin: WAL-401 85-21.

28 E.K. Storms: "A Critical Review of Refractories" (AEC) Rept. No. LA-2942 (1964).

29 J.T. Norton and R.K. Lewis: NASA-CR-321 (1963).

30 I. Gadoff and J.P. Nielsen: J. Metals 5 (1953) 248.

31 R.I. Bickerdike and G. Hughes: J.Less-Common Metals 1 (1959) 42.

32 J.Farr:Unpublished Work Quoted by E.K.Storms, LAMS-2674,(1962).

33 F.Benesovsky and E. Rudy: Planseeber.Pulvermet., 8 (1960) 66.

34 K.I. Portnoi, Yu.W.Levinski, W.I.Fadejeva: Akad. nauest. Nauk SSSR, nauest. Tekhn.Nauk, Metallurgija i Toplivo 2 (1961) 147.

35 R.G. Avarbe, A.L. Augustinnik, Yu.N.Vilk, Yu.D.Konrashov, S.S. Nikonskii, Yu.A.Omelchenko, and S.S.Ordanyan: Russian J. Appl. Chem., 35 (1962) 1899.

36 K. Becker and F. Ebert. Z. Physik., 31 (1925) 368.

37 G. Agte and H. Alterthum: Z. Tech. Physik, 11 (1930) 182.

38 D.G. Cotter and J.A. Kohn, J.Amer.Ceram.Soc., 37 (1954) 441.

39 N.H. Krikorian: Work quoted by C.K. Storms - See Ref. 32.

40 H.Nowotny and R. Kieffer: Metallforschung, 2 (1947) 257.

REFERENCES (Cont.)

41 J.T. Norton and A.L. Mowry: Trans AIME, 185 (1949) 133.

42 M.T. Tombrel, Plansee Proc., Reutte-Tirol (1955) 205.

43 A.E. Kovalski and E.J. Vrscheschi Tverdyje Splavy, 1 (1959) 305.

44 H.Nowotny, R.Kieffer, F.Benesovsky and G.Brukl: Mh.Chem. 90 (1959) 86.

45 H. Nowotny, F.Benesovsky and R.Kieffer: Planseeber.Pulvermet. 7 (1959) 78.

46 H. Nowotny, R.Kieffer, F. Benesovsky, G. Brukl and E.Rudy: Mh.Chem., 90 (1959) 669.

47 E. Rudy, H. Nowotny, F.Benesovsky, R.Kieffer and A.Neckel: Mh. Chem., 91 (1960) 176.

48 R.Kieffer and F.Benesovsky: "Hartstoffe" Springer-Verlag, Vienna (1963).

49 E.Rudy, St. Windisch and Y.A. Chang: AFML-TR-65-2, Part I, Vol. I, (Jan 1965).

50 W.D. Heetderks, E. Rudy and T. Eckert: AFML-TR-65-2, Part III, Vol. I, (April 1965).

51 Y.A. Chang: AFML-TR-65-2, Part IV, Vol. I (June 1965).

DOCUMENT CONTROL DATA - R&D

(Security classification of title, body of abstract and indexing annotation must be entered when the overall report is classified)

1 ORIGINATING ACTIVITY (Corporate author): Materials Research Laboratory, Aerojet-General Corporation, Sacramento, California	2a REPORT SECURITY CLASSIFICATION: Unclassified; 2b GROUP: N.A.

3 REPORT TITLE: Ternary Phase Equilibria in Transition Metal-Boron-Carbon-Silicon Systems
Part II. Ternary Systems, Volume IV. The Ti-Zr-C, Ti-Hf-C, and Zr-Hf-C Systems

4 DESCRIPTIVE NOTES (Type of report and inclusive dates):

5 AUTHOR(S) (Last name, first name, initial): Brukl, C. E.; Harmon, David P.

6 REPORT DATE: January 1966	7a TOTAL NO OF PAGES: 80	7b NO OF REFS: 51
8a CONTRACT OR GRANT NO: AF 33(615)-1247	9a ORIGINATOR'S REPORT NUMBER(S): AFML-TR-65-2 Part II. Vol. IV.	
b PROJECT NO: 7350		
c Task No. 735001	9b OTHER REPORT NO(S) (Any other numbers that may be assigned this report): N.A.	

10 AVAILABILITY/LIMITATION NOTICES: This document is subject to special export controls, and each transmittal to foreign governments or foreign nationals may be made only with prior approval of Metals & Ceramics Div., AF Materials Laboratory, Wright-Patterson AFB, Ohio.

11 SUPPLEMENTARY NOTES:	12 SPONSORING MILITARY ACTIVITY: AFML (MAMC) Wright-Patterson AFB, Ohio 45433

13 ABSTRACT

Solid-state sections of the ternary Ti-Zr-C and Ti-Hf-C systems were investigated; the complete Zr-Hf-C system was studied from 1600°C to melting using X-ray, DTA, melting point, and metallographic techniques on chemically analyzed alloys. A complete phase diagram for the Zr-Hf-C system for temperatures above 1600°C was established. The hafnium metal used contained 4 At.% zirconium. The Ti-Zr-C system contains a miscibility gap in the monocarbide region; the miscibility gap is completely closed at temperatures above approximately 2150°C. A miscibility gap is also present in the Ti-Hf-C system in the monocarbide region; complete solid solubility exists between the binary monocarbides at temperatures above approximately 2050°C. The Zr-Hf-C system contains a high melting, continuous monocarbide-solid-solution in a carbon defect lattice. The α-hafnium phase is stabilized toward higher temperatures by carbon; this phase shows a moderate solubility for carbon and zirconium. One four-phase reaction plane is present in the metal-rich portion of the ternary diagram. The results of these investigations are described and discussed; application possibilities are briefly mentioned.

DD FORM 1473

Unclassified
Security Classification

Unclassified

KEY WORDS	LINK A		LINK B		LINK C	
	ROLE	WT	ROLE	WT	ROLE	WT
Ternary Carbide High Temperature Phase Equilibria						

INSTRUCTIONS

1. **ORIGINATING ACTIVITY:** Enter the name and address of the contractor, subcontractor, grantee, Department of Defense activity or other organization (corporate author) issuing the report.

2a. **REPORT SECURITY CLASSIFICATION:** Enter the overall security classification of the report. Indicate whether "Restricted Data" is included. Marking is to be in accordance with appropriate security regulations.

2b. **GROUP:** Automatic downgrading is specified in DoD Directive 5200.10 and Armed Forces Industrial Manual. Enter the group number. Also, when applicable, show that optional markings have been used for Group 3 and Group 4 as authorized.

3. **REPORT TITLE:** Enter the complete report title in all capital letters. Titles in all cases should be unclassified. If a meaningful title cannot be selected without classification, show title classification in all capitals in parenthesis immediately following the title.

4. **DESCRIPTIVE NOTES:** If appropriate, enter the type of report, e.g., interim, progress, summary, annual, or final. Give the inclusive dates when a specific reporting period is covered.

5. **AUTHOR(S):** Enter the name(s) of author(s) as shown on or in the report. Enter last name, first name, middle initial. If military, show rank and branch of service. The name of the principal author is an absolute minimum requirement.

6. **REPORT DATE:** Enter the date of the report as day, month, year, or month, year. If more than one date appears on the report, use date of publication.

7a. **TOTAL NUMBER OF PAGES:** The total page count should follow normal pagination procedures, i.e., enter the number of pages containing information.

7b. **NUMBER OF REFERENCES:** Enter the total number of references cited in the report.

8a. **CONTRACT OR GRANT NUMBER:** If appropriate, enter the applicable number of the contract or grant under which the report was written.

8b, 8c, & 8d. **PROJECT NUMBER:** Enter the appropriate military department identification, such as project number, subproject number, system numbers, task number, etc.

9a. **ORIGINATOR'S REPORT NUMBER(S):** Enter the official report number by which the document will be identified and controlled by the originating activity. This number must be unique to this report.

9b. **OTHER REPORT NUMBER(S):** If the report has been assigned any other report numbers (either by the originator or by the sponsor), also enter this number(s).

10. **AVAILABILITY/LIMITATION NOTICES:** Enter any limitations on further dissemination of the report, other than those imposed by security classification, using standard statements such as:

(1) "Qualified requesters may obtain copies of this report from DDC."

(2) "Foreign announcement and dissemination of this report by DDC is not authorized."

(3) "U. S. Government agencies may obtain copies of this report directly from DDC. Other qualified DDC users shall request through _____."

(4) "U. S. military agencies may obtain copies of this report directly from DDC. Other qualified users shall request through _____."

(5) "All distribution of this report is controlled. Qualified DDC users shall request through _____."

If the report has been furnished to the Office of Technical Services, Department of Commerce, for sale to the public, indicate this fact and enter the price, if known.

11. **SUPPLEMENTARY NOTES:** Use for additional explanatory notes.

12. **SPONSORING MILITARY ACTIVITY:** Enter the name of the departmental project office or laboratory sponsoring (paying for) the research and development. Include address.

13. **ABSTRACT:** Enter an abstract giving a brief and factual summary of the document indicative of the report, even though it may also appear elsewhere in the body of the technical report. If additional space is required, a continuation sheet shall be attached.

It is highly desirable that the abstract of classified reports be unclassified. Each paragraph of the abstract shall end with an indication of the military security classification of the information in the paragraph, represented as (TS), (S), (C), or (U).

There is no limitation on the length of the abstract. However, the suggested length is from 150 to 225 words.

14. **KEY WORDS:** Key words are technically meaningful terms or short phrases that characterize a report and may be used as index entries for cataloging the report. Key words must be selected so that no security classification is required. Identifiers, such as equipment model designation, trade name, military project code name, geographic location, may be used as key words but will be followed by an indication of technical context. The assignment of links, rules, and weights is optional.

Unclassified
Security Classification

UNCLASSIFIED

UNCLASSIFIED